Galactic Cosmic rays from Supernova Remnants: II Shock Acceleration of Gas and Dust

Donald C. Ellison
Department of Physics, North Carolina State University,
Box 8202, Raleigh NC 27695, U.S.A.
don_ellison@ncsu.edu

Luke O'C. Drury
Dublin Institute for Advanced Studies, School of Cosmic Physics,
5 Merrion Square, Dublin 2, IRELAND
ld@cp.dias.ie

Jean-Paul Meyer
Service d'Astrophysique, CEA/DSM/DAPNIA
Centre d'Etudes de Saclay, 91191 Gif-sur-Yvette, FRANCE
meyer@sapvxb.saclay.cea.fr

Submitted to the *Astrophysical Journal,* October 8, 1996

Revised, January 20, 1997

Accepted, January 24, 1997

ABSTRACT

We present a quantitative model of galactic cosmic ray (GCR) origin and acceleration, wherein a mixture of interstellar and/or circumstellar gas and dust is accelerated by a supernova remnant (SNR) blast wave. The gas and dust are accelerated simultaneously, but differences in how each component is treated by the shock leaves a distinctive signature which we believe exists in the cosmic ray composition data. A re-examination of the detailed GCR elemental composition, presented in a companion paper, has led us to abandon the long held assumption that GCR abundances are somehow determined by first ionization potential (FIP). Instead, volatility and mass (presumably mass-to-charge ratio) seem to better organize the data: among the volatile elements, the abundance enhancements relative to solar increase with mass (except for the slightly high H/He ratio); the more refractory elements seem systematically overabundant relative to the more volatile ones in a quasi-mass-independent fashion. If this is the case, material locked in grains in the interstellar medium must be accelerated to cosmic ray energies more efficiently than interstellar gas-phase ions. Here we present results from a nonlinear shock model which includes (i) the direct acceleration of interstellar gas-phase ions, (ii) a simplified model for the direct acceleration of weakly charged grains to

$\sim$ 100 keV/amu energies, simultaneously with the acceleration of the gas ions, (iii) the energy losses of grains colliding with the ambient gas, (iv) the sputtering of grains, and (v) the simultaneous acceleration of the sputtered ions to GeV and TeV energies. We show that the model produces GCR source abundance enhancements of the volatile, gas-phase elements, which are an increasing function of mass, as well as a net, mass independent, enhancement of the refractory, grain elements over protons, consistent with cosmic ray observations. We also investigate the implications of the slightly high H/He ratio. The GCR ^{22}Ne excess may also be accounted for in terms of the acceleration of ^{22}Ne-enriched pre-SN Wolf-Rayet star wind material surrounding the most massive supernovae. We also show that cosmic ray source spectra, at least below $\sim 10^{14}$ eV, are well matched by the model.

Subject headings: Cosmic rays: general — particle acceleration — shock waves — interstellar medium

1. INTRODUCTION

The galactic cosmic ray source (GCRS) composition is relatively well determined at energies of a few GeV per nucleon. It is taken here to mean the relative values of the differential energy fluxes of the various nuclear species, each measured at the same energy per nucleon of order a few GeV/A (A is the nuclear mass number), and after applying "standard" corrections to the observed composition for solar modulation and interstellar propagation. Implicit in this is the assumption that all species have essentially identical energy spectra at source when plotted as functions of energy per nucleon, at least in the GeV range where good composition data can be obtained; observationally this does seem to be approximately the case (e.g., Swordy 1993; Shibata 1995). We note in passing that, whatever the validity of this assumption for the nuclear species, cosmic ray electrons have very different spectra and may, in fact, have entirely different origins (see Berezinskii et al. 1990 for a detailed account of cosmic ray physics).

If we accept these caveats, the resulting composition data show very interesting features. These have been discussed in detail in a companion paper by Meyer, Drury, and Ellison (1997; hereafter Paper I). We now summarize its conclusions. As compared to solar photospheric composition, the GCRS composition is characterized by a general overabundance of heavier elements relative to H and He, and by a fine structure among the heavy elements. This fine structure is primarily governed by atomic, not nuclear, physics; in particular, it does not at all correspond to fresh supernova nucleosynthesis products; (there exists, however, a ^{22}Ne, ^{12}C , ^{16}O-rich component in GCRs, suggesting the acceleration of some Wolf-Rayet wind material). The data indicate that the relevant atomic physics parameter could be either the first ionization potential (FIP), which controls the neutral or ionized state of each element in a $\sim 10^4$ K gas, or the element volatility (i.e., its condensation temperature, $T_{\rm c}$), which controls the element's ability to condense into solid compounds. For most elements, values of FIP and $T_{\rm c}$ are anti-correlated, so it is not easy to tell which of these two parameters shapes the GCRS composition. In any case, *either* the easily ionized low-FIP elements, *or* the easily condensed high-$T_{\rm c}$ elements, are found enhanced by a factor of order 5 relative to the other heavy elements (and ~ 30 relative to H).

Most studies to date have considered the FIP hypothesis, largely by analogy with the situation in the outer solar atmosphere, in which the solar coronal gas, the solar wind, and the ∼MeV solar energetic particles have undoubtedly a composition biased according to FIP. This bias implies some ion-neutral fractionation in the underlying cool, $\sim$ 7000 K chromospheric gas, in which neutrals and ions coexist: chromospheric ions must rise into the corona more efficiently than chromospheric neutrals. If FIP also determines the composition of GCRs, the cosmic rays must consist of injected ∼MeV stellar energetic particles, originating in F to M later-type stars possessing a neutral, cool chromosphere similar to that of the Sun, and then later preferentially reaccelerated to GeV and TeV energies by supernova shocks (Meyer 1985).

Fortunately, however, a few elements do *not* fit in the general anti-correlation between FIP and $T_{\rm c}$, and these can be used to lift the degeneracy and decide which of the two parameters is

relevant; these are low-FIP volatile elements (especially Na, Ge, Pb) and high-FIP refractories (P). These crucial elements are, unfortunately, not among those whose GCRS abundance is easiest to determine! But, with the steady progress over the past years, it has now become apparent that all four key ratios Na/Mg, P/S, Ge/Fe, Pb/Pt point towards volatility, not FIP, as the relevant parameter.

In Paper I, we have shown that all the GCRS composition data are remarkably well ordered in terms of two specific behaviors for the volatile and the refractory elements: (i) Among the volatile elements, the abundance enhancements strongly increase with element mass A; only hydrogen does not entirely fit into the pattern. We believe this reflects an increase of the acceleration efficiency with the element mass-to-charge ratio A/Q, i.e., with its rigidity at a given velocity; in any ionization model, indeed, A/Q is a roughly monotonically increasing function of the mass A (Q is the charge number). The low GCRS abundances of H, He, and N can be interpreted in this framework. (ii) The refractory elements are all enhanced relative to volatiles; but this enhancement is approximately the same for all refractories, i.e., it has *little or no* mass-dependence (see Figure 1).

This is a very surprising result. It is quite clear from UV, IR, and visible observations that the refractory elements are largely locked into solid dust grains in most of the interstellar medium (ISM) (e.g., Cardelli 1994; Sembach and Savage 1996; Savage and Sembach 1996), as well as in supernova ejecta (e.g. Lucy et al. 1989, 1991; Dwek et al. 1992), and in stellar, and especially Wolf-Rayet star, wind envelopes (e.g. Bode 1988; Gehrz 1991; van der Hucht and Hidayat 1991; van der Hucht and Williams 1995). Clearly, the GCRS composition features suggest a preferential acceleration of those elements locked in grains in most of the ISM and stellar ejecta (refractories), relative to the gas-phase elements (volatiles). This leads to the idea of a preferential acceleration of grain erosion products in supernova shocks, an idea which had been earlier approached, along two lines. Cesarsky and Bibring (1980) and Bibring and Cesarsky (1981) considered the destruction of grains after their free crossing of the shock, followed by stochastic acceleration of the grain destruction products. Epstein (1980), on the other hand, considered a preferential acceleration of the entire grains themselves, followed by their erosion, with the refractory grain erosion products keeping the high velocity first acquired by the grain (see Paper I for a fuller discussion).

It is this second line that we want to reexamine in this paper, in the light of the above, specific composition features, and of modern nonlinear (i.e., smoothed) shock acceleration theories. In this approach, we are encouraged by three basic observations: First, if particles with the same energy per nucleon are considered, smoothed shock models predict an increased particle acceleration efficiency for increased particle rigidity, i.e., A/Q ratio, because higher rigidity ions can diffuse further back upstream of the shock than low A/Q particles at the same energy per nucleon. Hence, high A/Q particles "see" a larger velocity difference and are more easily injected to suprathermal energies (e.g., Eichler 1979,1984; Ellison and Eichler 1984). This effect fits qualitatively with the mass dependence of the volatile, gas-phase element enhancements. Second, weakly charged grains can behave as extremely high A/Q ions, and thus get very efficiently injected and accelerated provided they obtain similar energies per nucleon to protons when first shock heated. Third, if the refractory

elements are, at the early crucial stage, accelerated as part of grains, their own A/Q plays no role in this acceleration stage, so that the approximate mass *in*dependence of their GCRS enhancements is not surprising.

In a way, this approach represents a synthesis between earlier fits of the global enrichment of heavier elements, especially relative to H, He, but which could not fit the fine structure of the heavy element composition, such as the Mg/Ne ratio (Ellison 1981; Ellison, Jones and Eichler 1981; Cesarsky, Rothenflug and Cassé 1981), and of approaches which used atomic physics to explain this fine structure (FIP, or volatility), but could not account for the low H and He abundances (Meyer 1985).

Leaving the observational study of the GCR composition, theoretical ideas on particle acceleration in shock waves have been developed to the point where quite sophisticated models are now routinely calculated. In this paper, we calculate expected source composition and spectral shapes of the GCRs, using a Monte Carlo model of cosmic ray acceleration at SNR shocks (e.g. Jones and Ellison 1991; Ellison 1993) including both interstellar gas and "grains." The shock model includes nonlinear effects from shock smoothing and a parameterized description of injection from the thermal background for any ion species or grain. It yields both the spectral shapes and absolute abundances of various species of cosmic rays. To this we have added a simple model of grain deceleration, sputtering of individual atoms off grains, and acceleration of sputtered ions to cosmic ray energies, yielding a first principles estimate of the refractory element/hydrogen ratio in cosmic rays.

While protons and helium ions are treated self-consistently and contribute to the shock smoothing, the other gas-phase ions and grains are treated as test particles, and are accelerated by the shock as smoothed by hydrogen and helium. Despite the approximations that must be made for such a complex calculation, we find *excellent agreement with observations* for both the spectral shape and the relative abundances of the various nuclear components, at least above a few GeV, where solar modulation is no longer important, and below the observed "knee" in the GCR spectrum and the Lagage and Cesarsky (1983) limit at $\sim 10^{14-15}$ eV (also Prishchep and Ptuskin, 1981). We believe this is the first attempt to simultaneously and self-consistently address the intensity and shape of the major cosmic ray components using a mixture of interstellar gas and dust.

2. MODEL ASSUMPTIONS

The hypothesis we wish to test is that the bulk of the GCRs at energies below the so-called "knee" at $\sim 10^{15}$ eV are accelerated by the forward shock waves associated with supernova remnants. The main arguments in favor of a SNR origin for the GCRs are that it is very hard to think of any other possible acceleration sites with adequate power (although stellar winds might be sufficient) (e.g. Axford 1981), and that SNRs are known from their radio synchrotron emission to accelerate electrons to cosmic ray energies (e.g., Reynolds and Ellison 1992). We assume the

forward shocks in the Sedov phase are mainly responsible for producing cosmic rays. While inner reverse shocks exist in the early remnant phases, the forward shocks are much longer lived and contain more energy. In addition, cosmic rays accelerated when the remnant is small suffer strong adiabatic losses making later stages more important(e.g., Drury and Keane 1995). The forward shocks accelerate mainly ambient interstellar material, although recent calculations of the Raleigh-Taylor instability in *young* SNRs (Jun & Norman 1996) suggest that some clumps of fast-moving ejecta may actually punch through the outer shock. However, there are good reasons to believe that these are relatively minor effects (see Drury and Keane 1995).

In addition, in diffusive shock acceleration (see Drury 1983; Völk 1984; Blandford and Eichler 1987; Berezhko and Krymsky 1988; Jones and Ellison 1991 for reviews), we have a plausible mechanism for producing energetic particles and one which has been observationally verified to work at heliospheric shocks under plasma conditions quite similar to those of interstellar shocks (e.g., Ellison, Möbius, and Paschmann 1990; Baring et al. 1995, although of course at much lower energies; but this merely reflects the small size and short life-time of heliospheric shocks). In its simplest test particle version, this mechanism predicts that all particles accelerated in a given shock will have identical power-law spectral shapes in momentum regardless of their charge (Krymsky 1977; Axford et al. 1977; Bell 1978; Blandford and Ostriker 1978). The spectra are naturally considered to be momentum spectra, rather than energy or velocity spectra say, because the basic acceleration process involves the change in momentum when switching from the upstream to the downstream reference frame.

However, at a more sophisticated level, where the reaction of the accelerated particles on the shock structure is considered [i.e. the upstream flow is slowed gradually (smoothed) by the pressure of backstreaming energetic ions before making an abrupt transition to the downstream state], the spectra are no longer exact power-laws, and different ion species are treated differently (e.g., Eichler 1984; Ellison and Eichler 1984). We note that if SNR shocks do indeed power GCRs, the power required ($\gtrsim 10\%$ of the total kinetic energy of SNR ejecta) implies that reaction effects of the cosmic rays on the shocks must be important. These effects produce different spectral shapes (in the range where all particles are not fully relativistic) and different injection and acceleration efficiencies for different ion species, with the ion rigidity and thermal speed becoming the important distinguishing parameters. In essence, the question which concerns us in this paper is whether the differences in the spectral shapes and absolute intensities for different elements, which inevitably result from this modification of the shock by reaction effects (Ellison 1993), combined with the acceleration and destruction of grain material, can explain in a quantitative way the observed features of the GCR composition. We find the answer to be yes, provided that charged grains and gas ions of the same rigidity act similarly in the shock acceleration process.

2.1. Spectra and Injection in Modified Shocks

While many different SNR shocks of varying ages, sizes, and strengths undoubtedly contribute to the observed cosmic ray flux, we only model single, steady-state shocks (of varying parameters) and leave more complex models for later work.

Let us consider a steady, plane-parallel, modified shock which we take to be propagating in the x-direction. The flow velocity profile, $U_{\rm x}(x)$, will then have a form similar to that indicated in Figure 2 by either the solid, dashed, or dot-dashed lines. At energies (or momenta) high enough for the diffusion approximation to be valid, the isotropic part of the phase space density, $f_\alpha(x,p)$, for particles of species α at position x and momentum p satisfies the well-known equation (e.g., Drury 1983)

$$U\frac{\partial f_\alpha}{\partial x} = \frac{\partial}{\partial x}\left[\kappa_\alpha(p,x)\frac{\partial f_\alpha}{\partial x}\right] + \frac{1}{3}\frac{\partial U}{\partial x}p\frac{\partial f_\alpha}{\partial p}\ , \tag{1}$$

where κ_α is the xx-component of the diffusion tensor for species α and is expected to be a rather strongly increasing function of momentum p. At energies close to thermal energies the diffusion approximation is no longer applicable, however, the same basic physics can easily be handled by Monte-Carlo simulations of the particle scattering off magnetic scattering structures embedded in the plasma flow (e.g., Ellison and Eichler 1984; Ellison, Jones, and Reynolds 1990; Jones and Ellison 1991). This computational model can be extended down to thermal energies and used to give a description of the particle distribution functions through the collisionless shock structure and of the shock itself. While it is certainly true that the detailed micro-physics of the collisionless shock structure is far more complicated than this simple Monte Carlo model, the results do seem to be in good agreement with heliospheric observations and with more detailed hybrid simulations (Ellison, Möbius, and Paschmann 1990; Ellison et al. 1993; Baring et al. 1995, 1997). Perhaps the best way to think of it is that this model provides a physically motivated means of estimating the relative rate at which different species will be injected and accelerated in a strong collisionless shock, and one which agrees with such observational evidence as is available for heliospheric shocks.

If high-energy particles can be removed from the system, either through a so-called upstream free-escape boundary (FEB), or simply by escaping when they reach a certain maximum momentum, it is possible to construct completely steady solutions, regardless of Mach number, in which the shock modification is self-consistently determined by the pressure of the accelerated particles. Such shock structures are shown in Figure 2. Full details and extensive comparisons with observations of heliospheric shocks can be found in the papers just mentioned as well as Ellison, Jones, and Reynolds (1990) and Ellison, Baring, and Jones (1995).

One point we wish to make is that, even if the shock structure is steady and the same for all species, the nonlinear effects of shock smoothing imply that species with differing diffusion coefficients will, in general, be accelerated differently and develop different spectra. However, we expect that the scattering mean free paths of the various species will be determined purely by the magnetic rigidity of each species, and thus, in the relativistic limit, all particles of a given rigidity

will have the same diffusion coefficient. This assumes, of course, that other physical constraints, such as the time available for acceleration being large compared to the particle gyroperiod, are satisfied. Spectral differences occur at nonrelativistic energies because different mass particles of the same rigidity have different speeds, and this results in a change in injection efficiency, and the resulting change in absolute accelerated particle intensities persists into the relativistic regime where the spectral shapes become the same.[1] More precisely, we define the rigidity of species α as

$$R = \frac{cp}{Q_\alpha e} = \frac{m_\mathrm{p} c^2}{e} \left(\frac{A}{Q}\right)_\alpha \beta\gamma \tag{2}$$

(with units of Volts in the SI system), where c is the velocity of light *in vacuo*, e is the electronic charge, m_p is the proton mass, $m_\alpha = A_\alpha m_\mathrm{p}$ is the rest mass of species α with A_α nucleons, Q_α is its charge number, β is the particle's v/c and γ is its Lorentz factor. The particle velocity is then

$$v = \left[1 + \left(\frac{m_\alpha c}{p}\right)^2\right]^{-1/2} = c\left[1 + \left(\frac{A_\alpha m_\mathrm{p} c^2}{Q_\alpha e R}\right)^2\right]^{-1/2} . \tag{3}$$

In a magnetic field, B, the gyroradius of the particle in SI units is $r_\mathrm{g} = p/(Q_\alpha e B) = R/(cB)$, and we expect from quasi-linear theory that the mean free path will be $\lambda(R) \sim r_\mathrm{g}/I(R)$, where $I(R)$ is the dimensionless power in magnetic field irregularities on length scales of order r_g (e.g., Drury 1983). In all that follows, we assume that $I(R)$ is independent of rigidity and position relative to the shock and write $\lambda = \eta r_\mathrm{g}$. The so-called strong scattering Bohm limit obtains when $\eta \sim 1$.

Thus the corresponding spatial diffusion coefficient will be

$$\kappa_\alpha = \frac{\lambda(R) v}{3} = \frac{c r_\mathrm{g} \eta}{3}\left[1 + \left(\frac{A_\alpha m_\mathrm{p} c^2}{Q_\alpha e R}\right)^2\right]^{-1/2} , \tag{4}$$

which, for non-relativistic velocities, reduces to

$$\kappa_\alpha = \frac{\eta}{3}\frac{e}{m_\mathrm{p} c^2}\frac{1}{B}\left(\frac{Q}{A}\right)_\alpha R^2 = \frac{\eta}{3}\frac{m_\mathrm{p} c^2}{e}\frac{1}{B}\left(\frac{A}{Q}\right)_\alpha \beta^2 . \tag{5}$$

We see that particles with the same rigidity but different values of $(A/Q)_\alpha$ will have different diffusion coefficients in the sub-relativistic region and, therefore, different diffusion lengths in the shock precursor. Since the diffusion length in the precursor is $L_{\mathrm{D},\alpha} \sim \kappa_\alpha / U_\mathrm{x}(x) \propto \lambda_\alpha v_\alpha$, the ratio of diffusion lengths of species α to protons, at fixed energy per nucleon, is simply

$$\frac{L_{\mathrm{D},\alpha}}{L_{\mathrm{D,p}}} \propto \left(\frac{A}{Q}\right)_\alpha . \tag{6}$$

[1] As we report later in the paper, our results show that spectral differences between iron and hydrogen/helium are noticeable well into the relativistic regime.

If the shock is smooth rather than discontinuous (cf., Figure 2) as will always be the case in nonlinear shock acceleration if κ is an increasing function of energy, ions with large A/Q will diffuse further upstream than protons of the same energy per nucleon (provided both are nonrelativistic). These ions will be turned around against a more rapid upstream flow, will receive a larger energy boost for each shock crossing, and will be accelerated more efficiently and obtain a flatter spectrum than protons (e.g., Ellison, Jones, and Eichler 1983; Ellison and Eichler 1984). Recent specific observational support for this effect in anomalous cosmic rays has been reported by Cummings and Stone (1996). While the differences in A/Q may be small for atoms, grains can have huge A/Q's ($\sim 10^{4-8}$). If all particles become relativistic, the term in square brackets in Eq. (4) goes to one and the differences in κ vanish, but the intensities of the spectra of various species, acquired when they were nonrelativistic, will be different, and this difference persists to the highest energies obtained.

It is important to note that this conclusion is based on our assumption of a steady state. The longer diffusion lengths of heavy ions also result in longer acceleration *times* to a given energy per nucleon. If the shock has a finite age, the acceleration of heavy ions, and particularly grains, may cutoff before protons.

2.2. Acceleration of Dust Grains

We now revive an old suggestion of Epstein (1980) that charged dust grains could be efficiently accelerated by shocks to produce cosmic rays (see also Meyer 1993). A related idea, that grain destruction products could be stochastically accelerated behind shocks, was presented by Cesarsky and Bibring (1980) and Bibring and Cesarsky (1981). The basic idea of Epstein (1980) was that the dust grains could behave like ions of very large mass to charge ratio, thus large rigidity, and should therefore be relatively efficiently accelerated to velocities where they are eroded by sputtering. The sputtered grain material will have the velocity of the parent grain which can be well above thermal. If the sputtering occurs in the upstream region the sputtered products (i.e., refractory elements) will be carried back into the shock and further accelerated to cosmic ray energies with higher net efficiency than the gas-phase thermal protons and volatile element ions. Of course, material which is sputtered from the grains downstream of the shock is mainly carried away and lost from the system because the sputtered ions are, on average, many more mean free paths downstream from the shock then the parent grain.

Small grains in a plasma will be charged by a number of processes. In the absence of any other effects, they acquire a negative charge because the thermal electron flux impinging on their surface is higher than the ion flux; this tends to charge the grain to a negative potential of order $-2.5kT/e$ where T is the plasma temperature (e.g., Spitzer 1978). However a number of competing processes lead to electron loss from the grain. A significant UV photon flux can charge the grain by the photoelectric effect to a positive potential corresponding to the difference between the photon energy and the work function of the grain surface. If the grain is moving through the plasma, neutral atom and ion impacts on the grain surface can lead to secondary electron emission which

also charges the grain positively. At $T > 10^5$K, the charging effect of the thermal electron flux is largely cancelled by the fact that the electrons themselves produce secondary electron emission. All of these processes, together with poorly known grain properties, make an exact determination of the grain charge impossible. What one can say with certainty is that a grain will only be uncharged very briefly, if at all, and that in general the potential of the grain will be of order 10 to 100 V (it is of course no coincidence that this is the characteristic energy range of atomic physics and electronic transitions). McKee et al. (1987) show in their Figure 6 some interesting model calculations of grain potentials under various assumptions.

It follows that if the grain potential is ϕ, the charge on a spherical grain is of order $q \sim 4\pi\epsilon_0 a\phi$, where a is a characteristic size of the grain (note that the grains will certainly not be perfect spheres; in fact the larger grains probably have a fractal structure). In terms of electronic charges this gives numerically

$$Q_{\rm G} = \frac{q}{e} \simeq 700 \left(\frac{a}{10^{-7}{\rm m}}\right)\left(\frac{\phi}{10{\rm V}}\right) \ . \tag{7}$$

The number of atoms in the grain will be of order $(a/10^{-10}{\rm m})^3$, or 10^9 for a 10^{-7}m size grain (or less if the grain has a very open fractal structure). If μ is the mean atomic weight of the grain atoms, the entire grain "atomic weight," $A_{\rm G}$, is $\mu(a/10^{-10}{\rm m})^3$. Thus the effective A/Q value for a grain is very large, of order

$$\left(\frac{A}{Q}\right)_{\rm G} \simeq 1.4\times 10^6 \mu \left(\frac{a}{10^{-7}{\rm m}}\right)^2 \left(\frac{\phi}{10{\rm V}}\right)^{-1} \ . \tag{8}$$

If the dust grain has velocity $\beta_{\rm G}c$ with $\beta_{\rm G} \ll 1$, then the magnetic rigidity of the grain is

$$R = \frac{cp}{q} = \frac{A_{\rm G} m_{\rm p} \beta_{\rm G} c^2}{Q_{\rm G} e} \simeq 10^9 \beta_{\rm G} \left(\frac{A}{Q}\right)_{\rm G} \quad {\rm V} \ , \tag{9}$$

where $p = \beta_{\rm G} c A_{\rm G} m_{\rm p}$ is the momentum of the grain. Numerically, the grain rigidity is

$$R \simeq 1.3\times 10^{15} \beta_{\rm G} \mu \left(\frac{a}{10^{-7}{\rm m}}\right)^2 \left(\frac{\phi}{10\,{\rm V}}\right)^{-1} \ {\rm V} \ . \tag{10}$$

Ultraviolet and optical extinction measurements indicate that the grain size distribution is quite broad extending from very small grains to an upper cutoff at $\sim 0.25\mu$m (e.g., Mathis, Rumpl, and Nordsieck 1977). The amount of total grain mass in particles with radii a or less, $M_{\rm G}(< a)$, goes roughly as $a^{1/2}$, so that nearly half of the total grain mass is in a relatively small range of sizes around $0.1\,\mu$m.

In general, supernova remnant shocks have velocities in the range 30 to $3000\,{\rm km\,s^{-1}}$ (e.g., Reynolds 1988). Let us consider a high Mach number shock of velocity $400\,{\rm km\,s^{-1}}$ which overtakes a dust grain in a typical interstellar hydrogen density, $n_{\rm H} \sim 1$ cm^{-3}. Relative to the post-shock gas, the grain will have a velocity of $\sim 300\,{\rm km\,s^{-1}}$ or $\beta_{\rm G} \sim 10^{-3}$, and thus a rigidity of about 10^{14} V if

it is 0.1 μm in size, is charged to a surface potential of 10 V, and is made of material with $\mu \sim 56$.[2]

Can dust grains be accelerated by SNR shocks? We assume that SNR shocks are capable of accelerating *protons* to energies of order 10^{14-15} eV, as suggested by theoretical arguments concerning shock acceleration (e.g., Blandford and Eichler 1987), is required if they are to account for the near constant slope of the observed proton spectrum up to the knee at $>10^{14}$ eV, and will certainly occur if SNRs do, in fact, accelerate *electrons* to $\sim 10^{14}$ eV, as has been claimed for SNR SN 1006 (Koyama et al. 1995; Reynolds 1996). If this is the case, three conditions must be met; (i) the magnetic field near the shock has to contain structures capable of scattering protons of rigidities up to 10^{14-15} V, (ii) the shock radius (i.e., the size of the acceleration region) must be considerably larger than a $\sim 10^{14-15}$ eV proton gyroradius, and (iii) the age of the remnant must be greater than the acceleration time to $\sim 10^{14-15}$ eV. Our fundamental assumption is: if relativistic protons of energy $> 10^{14}$ eV are being efficiently scattered and accelerated (i.e., are being scattered nearly elastically and isotropically in the local plasma frame), *then so should dust grains with the same rigidity*. There is however one vital difference. The dust grains, far from being relativistic, only have a velocity of order the shock velocity, at least initially. Since we also assume that the mean free path depends only on rigidity, not velocity, the diffusion coefficient of the grains is smaller than that of the relativistic protons with the same rigidity by a factor of the grain β, typically 10^{-3}.

For diffusive shock acceleration, the standard estimate of the acceleration time, $\tau_{\rm a}$, to a momentum p is

$$\tau_{\rm a} = \frac{3}{\Delta U} \int_{\rm p_i}^{\rm p} \left(\frac{\kappa_1}{U_1} + \frac{\kappa_2}{U_2} \right) \frac{dp'}{p'} \ , \tag{11}$$

where κ_1 (κ_2) is the upstream (downstream) diffusion coefficient parallel to the shock normal, U_1 (U_2) is the far upstream (downstream) flow speed measured in the shock frame, $\Delta U = U_1 - U_2$, and $p_{\rm i} \ll p$ is the injection momentum of the particle (e.g., Axford 1981). Using this, we can define the instantaneous acceleration time scale, $t_{\rm acc} = p/(dp/dt)$, as

$$t_{\rm acc} \simeq \frac{3}{\Delta U} \frac{\kappa_1}{V_{\rm sk}} (1 + gr) \ , \tag{12}$$

where $r = U_1/U_2$ is the shock compression ratio, $V_{\rm sk} = U_1$ is the shock speed, and we have taken $\kappa_2 = g\kappa_1$. The parameter g is expected to lie between 0 and 1 and will equal $1/r$ if the diffusion coefficient is inversely proportional to background density. We consider $g = 1/r$ a good approximation (see Ellison, Möbius, and Paschmann 1990) and will use this in the derivation which follows. We will also approximate $\Delta U = V_{\rm sk}(1 - 1/r) \sim V_{\rm sk}$ in the following expressions.

Therefore, using $\lambda = \eta r_{\rm g}$ and Eq. (8), the acceleration time scale of a nonrelativistic grain can

[2]While the value $\mu = 56$ only applies to pure iron grains, we have chosen it for simplicity. For silicate grains containing Mg, Si, Fe, and O, $\mu \sim 20$ to 30, but this factor of about two difference does not seriously influence the results that follow.

be written as

$$t_{\rm acc} \simeq 10^4 \eta \left(\frac{\mu}{56}\right) \left(\frac{a}{10^{-7}{\rm m}}\right)^2 \left(\frac{\phi}{10{\rm V}}\right)^{-1} \left(\frac{B}{3\mu{\rm G}}\right)^{-1} \left(\frac{V_{\rm sk}}{400\,\frac{\rm km}{\rm s}}\right)^{-2} \left(\frac{\beta_{\rm G}}{0.01}\right)^2 \ {\rm yr} \ . \tag{13}$$

Initially, the acceleration rate for grains with $v_{\rm G} \sim V_{\rm sk} = 400$ km s^{-1} (i.e., $\beta_{\rm G} \sim 0.0013$), is very fast, i.e., $t_{\rm acc} \simeq 200$ yrs for our standard grain parameters and assuming $\eta = 1$. Strictly speaking, Eq. (11) (which is based on diffusive acceleration theory) is inapplicable in this low velocity limit, but Monte-Carlo simulations (e.g., Ellison, Baring, and Jones 1995) have shown that it is quite accurate down to thermal energies. We have been working with the momentum acceleration time-scale, $p/(dp/dt)$; the kinetic energy acceleration time-scale, $E/(dE/dt)$, will be exactly half this, as long as the grains are non-relativistic and $E \propto p^2$.

An important constraint is that the age of the remnant, $t_{\rm SNR}$, is greater than the acceleration time and that the acceleration time is greater than the gyroperiod of the grain, $T_{\rm G} = 2\pi r_{\rm g}/v_{\rm G}$, so that the grain has time to spiral and scatter in the background magnetic field, i.e.,

$$T_{\rm G} \ll t_{\rm acc} < t_{\rm SNR} \ . \tag{14}$$

The gyroperiod of a nonrelativistic grain is

$$T_{\rm G} \simeq 10\mu \left(\frac{a}{10^{-7}\,{\rm m}}\right)^2 \left(\frac{\phi}{10\,{\rm V}}\right)^{-1} \left(\frac{B}{3\,\mu{\rm G}}\right)^{-1} \ {\rm yr} \ , \tag{15}$$

and

$$\frac{t_{\rm acc}}{T_{\rm G}} \simeq 20\eta \left(\frac{\beta_{\rm G}}{0.01}\right)^2 \left(\frac{V_{\rm sk}}{400\,\frac{\rm km}{\rm s}}\right)^{-2} \ , \tag{16}$$

so the left-half of eq. (14) is easily satisfied for $V_{\rm sk} \sim 400$ km s^{-1}, $\beta_{\rm G} = 0.01$, and $\eta = 1$. Therefore, it is reasonable to assume (as we do) that grains can interact collisionlessly by gyrating in the turbulent magnetic fields. At the beginning of the acceleration process, $t_{\rm acc}/T_{\rm G}$ can certainly be less than one but eq. (11) doesn't describe the acceleration rate in the first few crossings of the shock.

For the right-half of eq. (14), we use the standard Sedov solution (e.g., Lang 1980) for an explosion of initial energy, $E_{\rm SN}$, in a gas of density $\rho = 1.4 n_{\rm H} m_{\rm p}$, to estimate $V_{\rm sk}$ as a function of $t_{\rm SNR}$, i.e.,

$$V_{\rm sk} = \frac{2}{5}\xi \left(\frac{E_{\rm SN}}{\rho}\right)^{1/5} t_{\rm SNR}^{-3/5} \ , \tag{17}$$

where $\xi \sim 1.15$ (e.g., Shu 1992) and $n_{\rm H}$ is the hydrogen number density. Using this value of $V_{\rm sk}$ in eq. (13) we have

$$\frac{t_{\rm SNR}}{t_{\rm acc}} \simeq \frac{2}{\eta} \left(\frac{\mu}{56}\right)^{-1} \left(\frac{a}{10^{-7}\,{\rm m}}\right)^{-2} \left(\frac{\phi}{10\,{\rm V}}\right) \left(\frac{B}{3\,\mu{\rm G}}\right) \left(\frac{\beta_{\rm G}}{0.01}\right)^{-2} \times \left(\frac{n_{\rm H}}{1\,{\rm cm}^{-3}}\right)^{-2/5} \left(\frac{E_{\rm SN}}{10^{51}{\rm erg}}\right)^{2/5} \left(\frac{t_{\rm SNR}}{10^3{\rm yr}}\right)^{-1/5} \ , \tag{18}$$

demonstrating that the right-half of eq. (14) can also be satisfied.

An additional constraint for acceleration is that the diffusion length must be less than the shock radius, $R_{\rm sk}$, i.e.,

$$\frac{\kappa}{V_{\rm sk}R_{\rm sk}} < 1 \ , \tag{19}$$

or, using

$$R_{\rm sk} = \xi \left(\frac{E_{\rm SN}}{\rho}\right)^{1/5} t_{\rm SNR}^{2/5} \tag{20}$$

from the Sedov solution,

$$0.03\eta \left(\frac{\mu}{56}\right) \left(\frac{a}{10^{-7}\,{\rm m}}\right)^2 \left(\frac{\phi}{10\,{\rm V}}\right)^{-1} \left(\frac{B}{3\,\mu{\rm G}}\right)^{-1} \left(\frac{\beta_{\rm G}}{0.01}\right)^2 \left(\frac{n_{\rm H}}{1\,{\rm cm}^{-3}}\right)^{2/5} \times \left(\frac{E_{\rm SN}}{10^{51}{\rm erg}}\right)^{-2/5} \left(\frac{t_{\rm SNR}}{10^3{\rm yr}}\right)^{1/5} < 1 \ . \tag{21}$$

This is easily satisfied for the values of $\beta_{\rm G}$ we consider.

2.3. Loss Time Scales

The acceleration time-scale from shock acceleration has to be compared to the momentum loss time-scale due to frictional coupling of the grain to the background plasma to determine whether acceleration really occurs. There are two components to the frictional interaction. First, there is a component due to direct collisions of the grain with atoms or ions of the plasma. Since even for a 10^6 K gas, $v_{\rm G} \geq V_{\rm sk} > v_{\rm H,thermal}$, the collision rate is of order $n_{\rm H}a^2\beta_{\rm G}c$, where each collision reduces the grain momentum by a fraction of order $1.4/A_{\rm G}$ (assuming that collisions with hydrogen dominate and that helium increases the loss rate by about 40%). Grain-grain collisions may also be important but this process depends on the distribution of grain sizes, is highly uncertain, and is not expected to contribute much to momentum losses since grains contain a small fraction of the total mass of the ambient gas (K. Borkowski, private communication). Thus, neglecting grain-grain collisions, the momentum loss time-scale resulting from direct collisions, $t_{\rm loss,mom}$, is of order

$$t_{\rm loss,mom} \simeq \frac{A_{\rm G}}{1.4 n_{\rm H} a^2 \beta_{\rm G} c} \simeq 8\mu \left(\frac{a}{10^{-7}{\rm m}}\right) \left(\frac{n_{\rm H}}{1\,{\rm cm}^{-3}}\right)^{-1} \beta_{\rm G}^{-1}\ {\rm yr} \ , \tag{22}$$

and the ratio of this loss time-scale to the acceleration time-scale is

$$\frac{t_{\rm loss,mom}}{t_{\rm acc}} \simeq \frac{4\times10^{-6}}{\eta} \left(\frac{a}{10^{-7}{\rm m}}\right)^{-1} \left(\frac{n_{\rm H}}{1\,{\rm cm}^{-3}}\right)^{-1} \left(\frac{\phi}{10\,{\rm V}}\right) \left(\frac{B}{3\,\mu{\rm G}}\right) \left(\frac{V_{\rm sk}}{400\,\frac{\rm km}{\rm s}}\right)^2 \beta_{\rm G}^{-3} \ , \tag{23}$$

interestingly with no dependence on grain composition, μ.

Secondly, we have to consider the indirect drag on the grain resulting from long-range electrostatic interactions. It is easy to show (Draine and Salpeter, 1979) that these effects are less important than direct collisions and we neglect them in what follows. Therefore, from equation (23) we

conclude that losses become progressively more important as the grains are accelerated to higher velocities. This will quench the acceleration at the velocity where $t_{\rm acc} \sim t_{\rm loss,mom}$, i.e.,

$$\beta_{\rm G,max} \simeq 0.016 \eta^{-1/3} \left(\frac{V_{\rm sk}}{400\,\frac{\rm km}{\rm s}}\right)^{2/3} \left(\frac{a}{10^{-7}\,{\rm m}}\right)^{-1/3} \left(\frac{n_{\rm H}}{1\,{\rm cm}^{-3}}\right)^{-1/3} \left(\frac{\phi}{10\,{\rm V}}\right)^{1/3} \left(\frac{B}{3\,\mu{\rm G}}\right)^{1/3} \ , \qquad (24)$$

or

$$\beta_{\rm G,max} \simeq 0.016 \qquad (25)$$

for our standard parameters: $V_{\rm sk} = 400$ km s^{-1}, $\eta = 1$, $a = 10^{-7}$ m, $n_{\rm H} = 1$ cm^{-3}, $\phi = 10$ V, and $B = 3$ μG. So, the grain $\beta_{\rm G}$ can be increased from an initial value of order 10^{-3} to one of order 10^{-2}, with a rather weak dependence on the ambient density, magnetic field, and grain size.

This can be written in terms of the maximum energy per nucleon, i.e.,

$$\left(\frac{E}{A}\right)_{\rm G,max} \simeq 100 \eta^{-2/3} \left(\frac{V_{\rm sk}}{400\,\frac{\rm km}{\rm s}}\right)^{4/3} \left(\frac{a}{10^{-7}\,{\rm m}}\right)^{-2/3} \left(\frac{n_{\rm H}}{1\,{\rm cm}^{-3}}\right)^{-2/3} \times \left(\frac{\phi}{10\,{\rm V}}\right)^{2/3} \left(\frac{B}{3\,\mu{\rm G}}\right)^{2/3} \ {\rm keV} \ , \qquad (26)$$

So our standard parameters yield $(E/A)_{\rm G,max} \simeq 100$ keV, well above thermal energies. Of course this does not mean that all grains are accelerated by this amount, in fact, a distribution extending upwards from thermal energies will result with only a small fraction of grains obtaining the cutoff energy $(E/A)_{\rm G,max}$. In addition, as described above, the shock must be large enough and old enough for acceleration to these velocities to occur.

2.4. Grain Sputtering and Injection of Sputtered Material

The acceleration of grains has significant implications for grain erosion by sputtering. At the velocities indicated in equation (24), the sputtering process is quite uncertain and grains may even become transparent (e.g., Dwek 1987), but we assume that roughly 0.5 to 1% of collisions with ambient gas atoms result in the sputtering of an atom from the grain surface. On average, each such event reduces $A_{\rm G}$ by μ. Therefore, the grain destruction time-scale for collisional sputtering, $t_{\rm loss,sput} = A_{\rm G}/(dA_{\rm G}/dt)$, is approximately

$$t_{\rm loss,sput} \simeq \frac{100 A_{\rm G}}{n_{\rm H} a^2 \beta_{\rm G} c \mu} \ . \qquad (27)$$

Comparing $t_{\rm loss,sput}$ to the momentum-loss time-scale $t_{\rm loss,mom}$ for direct collisions with the same gas atoms (eq. 22), we get

$$\frac{t_{\rm loss,sput}}{t_{\rm loss,mom}} \simeq \frac{140}{\mu} \ , \qquad (28)$$

so that $t_{\rm loss,sput} \sim O(10) \times t_{\rm loss,mom}$ for $\mu \sim 20$. For instance, the larger grains ($a \sim 10^{-7}$ m) accelerated to $\beta_{\rm G} \sim 10^{-2}$, which have loss and acceleration time-scales of order 10^4 yr for $n_{\rm H} =$

1 cm^{-3}, have sputtering time scales of some 10^5 yr. The key point is that the acceleration time-scales are always shorter than the destruction time-scales. This means that the grain has time to diffuse back and forth between both sides of the shock before being destroyed. Thus, some of the sputtering must occur while the grain is in the upstream region ahead of the shock. These sputtered particles can then be advected into the shock as a seed population of energetic ions which can then be accelerated with high efficiency, if they do not lose too much energy to ionization and Coulomb collision losses while being advected from the sputtering site to the shock.

The accelerated dust grains will be distributed in the upstream region with a roughly exponential spatial distribution falling on a length-scale of order $\kappa/V_{\rm sk}$. The time-scale for the sputtered ion to be advected back to the shock, $t_{\rm ad}$, is thus $\kappa/V_{\rm sk}^2$ (note that the much smaller rigidity of the ion compared to the parent grain means that we can ignore the diffusion of the ion) and is thus of order $t_{\rm acc}/6$ (i.e. equation 12). If we consider grains accelerated to the point where the acceleration just balances the losses due to collisions (Eq. 24), which is where most of the sputtering occurs, the advection time-scale of the sputtered ions is

$$t_{\rm ad} \simeq 1.6 \times 10^3 \eta \left(\frac{\mu}{56}\right) \left(\frac{\beta_{\rm G}}{0.01}\right)^2 \left(\frac{a}{10^{-7}\,{\rm m}}\right)^2 \left(\frac{\phi}{10\,{\rm V}}\right)^{-1} \left(\frac{B}{3\,\mu{\rm G}}\right)^{-1} \left(\frac{V_{\rm sk}}{400\,\frac{\rm km}{\rm s}}\right)^{-2} {\rm yr}, \qquad (29)$$

typically ~ 2000 years for the larger, $a \sim 10^{-7}$ m, grains, but falling as the second power of the grain size for smaller grains. The corresponding advection length scale, $V_{\rm sk} t_{\rm ad}$, is of order of a parsec.

We must now estimate the losses of the sputtered ions on the advection time-scale. The ion is unlikely to be fully stripped, especially if of high nuclear charge. On ejection from the grain it will carry some electrons with it, and there will also be electron exchange with the atoms of the background plasma. The cross section for electron stripping or pick-up is of order $10^{-16}\,{\rm cm}^2$, so that in a medium of hydrogen number density $n_{\rm H} \sim 1\,{\rm cm}^{-3}$ and at a velocity of order $\beta_{\rm G} \sim 10^{-2}$, the time-scale for electron exchange is of order ~ 1 yr. Electrons will be stripped or picked-up until the kinetic energy of colliding electrons in the ion's frame is of the same order as the ion's ionization potential. In the case of a cold plasma, in which $\beta_{\rm e,th} \ll \beta_{\rm G}$ for virtually all thermal electrons in the Maxwell tail, this corresponds to ionization potentials of $\sim 25(\beta_{\rm G}/10^{-2})^2$ eV. For $\beta_{\rm G} \sim 10^{-2}$, this is of order the 1$^{\rm st}$, 2$^{\rm nd}$, or at most 3$^{\rm rd}$ ionization potential of all elements. Thus we expect the ions to have an effective charge Q^* of at most +3 and those elements with high first ionization potentials actually have a significant chance of becoming neutral atoms. Such neutrals, if formed, are no longer trapped by the magnetic field and move in a straight line until they again become ionized. If the charge exchange time-scale is of order one year, the displacement through this effect is of order 10^{14} m, substantially less than the size of the advection region except for the very smallest grains where it may be a significant effect.

The above estimates apply to a 10^4 K plasma, in the absence of steady photoionization. In a hot plasma consisting of ions with ionization potentials > 25 eV, the equilibrium charge is determined, not by the accelerated ion velocity $\beta_{\rm G}$, but by the thermal balance of the gas. This applies to a

10^6 K plasma, in which, e.g., accelerated Mg and Fe ions will reach effective charges of $Q^* \sim +8$ and +9, respectively.

The momentum loss time-scale of an ion with velocity $\beta_{\rm G,max}$, due to ionization energy loss and Coulomb collisions is

$$t_{\rm ion,loss} \sim 2000 \frac{\mu}{Q^{*2}} \left(\frac{\beta_{\rm G,max}}{10^{-2}} \right)^3 \left(\frac{n_e}{1\,{\rm cm}^{-3}} \right)^{-1} ({\rm ln}\Lambda)^{-1} \Psi^{-1} \ {\rm yr} \ , \tag{30}$$

in which $\Psi(v_{\rm G,max}/v_{\rm e,th})$ describes the decrease of the momentum loss rate in hotter plasmas, in which the thermal electron velocity $v_{\rm e,th}$ becomes comparable to the energetic ion velocity $v_{\rm G,max}$ (Spitzer 1962; Ryter et al. 1970). With $\ln \Lambda = O(20)$, $\mu = O(50)$, $Q^{*2} = O(4)$, $\Psi = 1$ for $T = 10^4$ K, and $Q^{*2} = O(100)$, $\Psi = 0.16$ for $T = 10^6$ K, we get $t_{\rm ion,loss} \sim 1000$ and ~ 300 yr for 10^4 K and 10^6 K gases. These figures are roughly comparable to, but somewhat smaller than the ~ 2000 yr advection time-scale we estimated for the larger grains, so that energy loss can be significant, especially for a hot ambient gas. However, the sputtering occurs throughout an extended region. This means that even for the largest grains, which have the most spatially extended distribution, those ions sputtered near the shock are advected into the shock before they have suffered significant energy losses. The surviving fraction can be estimated as $1 - \exp(-t_{\rm ion,loss}/t_{\rm ad}) \sim 1/2.5$ for $T = 10^4$ K and $\sim 1/7$ for $T = 10^6$ K for the largest grains, but it rapidly tends to 1 for smaller grains (Eq. 29). The actual importance of this loss, of course, also depends on the gas density. In the subsequent rough approach, we will neglect this loss, and assume that all of the sputtered ions are convected back to the shock.

2.4.1. Refractory Element Injection Rate

We are now in a position to estimate the suprathermal refractory element injection rate resulting from the sputtering of grains in the upstream region, followed by the advection of the resulting suprathermal ions into the shock. If the number density of thermal grains far upstream of the shock is $n_{\rm G}$, and the velocity spectrum of the accelerated grains at and downstream of the shock is of the form $N(v_{\rm G}) = N_0 (v_{\rm G}/v_0)^{-2}$ from an initial velocity $v_0 \sim 3U/4$ to a maximum velocity $v_{\rm G,max} \sim 10 v_0$, then

$$\int_{v_0}^{v_{\rm G,max}} N_0 \left(\frac{v_{\rm G}}{v_0} \right)^{-2} dv_{\rm G} \sim 4 n_{\rm G} \ , \tag{31}$$

or $v_0 N_0 \sim 4 n_{\rm G}$. Note that we have assumed that the shock has a compression $r = 4$ and the accelerated grain spectrum has the corresponding test-particle power law with index -2. While we have included all downstream grains (even thermal ones) in the power law spectrum, and our parameters, as well as the shape of the spectrum, will be modified substantially in our nonlinear models presented below, the following calculation is useful as a rough estimate of the injection efficiency.

To calculate the injection rate, we assume that the sputtering rate per grain is of order $0.01 n_{\rm H} a^2 v_{\rm G}$, and that the grains are exponentially distributed in the upstream region on a scale

$\kappa(v_{\rm G})/V_{\rm sk}$. Further assuming that the sputtered ions have the same velocity, $v_{\rm G}$, as the parent grain, we find the ion injection rate per unit surface area of the shock for ions with velocities between v and $v + dv$ is

$$I(v)dv \simeq \frac{\text{sputters}}{\text{unit time} \cdot \text{grain}} \times \frac{\text{grains in } dv}{\text{volume}} \times \text{scale length} \times dv \ , \tag{32}$$

that is,

$$I(v)dv \simeq [0.01 n_{\rm H} a^2 v] \left[N_0 \left(\frac{v}{v_0} \right)^{-2} \right] \left[\frac{\kappa(v)}{V_{\rm sk}} \right] dv, \qquad v_0 < v < 10 v_0 \ , \tag{33}$$

where we have dropped the subscript 'G' on velocity. Replacing N_0 with $4n_{\rm G}/v_0$, noting that $\kappa(v)/V_{\rm sk}^2 \simeq t_{\rm acc}/6$, and that $n_{\rm H} a^2 v \simeq A_{\rm G}/(1.4 t_{\rm loss,mom})$ (Eqs. 12 and 22), we obtain

$$I(v)dv \sim 5 \times 10^{-3} n_{\rm G} A_{\rm G} \frac{V_{\rm sk}}{v_0} \left(\frac{v}{v_0} \right)^{-2} \frac{t_{\rm acc}}{t_{\rm loss,mom}} dv \ . \tag{34}$$

Now, from equation (33), we see that, since $\kappa \propto v^2$ (Eq. 5), the injection rate rises as $I(v) \propto v$. The maximum value is obtained at $v_{\rm G,max} \sim O(10 v_0)$, where the acceleration time scale and the direct collisional momentum loss time-scales coincide, i.e., where $t_{\rm acc} \sim t_{\rm loss,mom}$. This implies that

$$I(v) \sim 5 \times 10^{-3} n_{\rm G} A_{\rm G} \frac{V_{\rm sk}}{v_0} \left(\frac{v_{\rm G,max}}{v_0} \right)^{-2} \frac{v}{v_{\rm G,max}} \ , \tag{35}$$

and thus the total injection rate of sputtered ions per unit surface area is

$$q_{\rm sput} = \int_{v_0}^{v_{\rm G,max}} I(v)dv \ \sim \ 5 \times 10^{-3} n_{\rm G} A_{\rm G} \frac{V_{\rm sk}}{v_0} \left(\frac{v_{\rm G,max}}{v_0} \right)^{-2} \frac{v_{\rm G,max}^2 - v_0^2}{2 v_{\rm G,max}} \ , \tag{36}$$

or

$$q_{\rm sput} \sim O(10^{-4}) n_{\rm G} A_{\rm G} V_{\rm sk} \ . \tag{37}$$

The quantity $n_{\rm G} A_{\rm G} V_{\rm sk}$ is the flux of nucleons contained in grain material coming from far upstream. This result can be interpreted as saying that, with a probability of order 10^{-4}, an atom in a dust grain will be sputtered as a suprathermal ion while in the upstream region and be convected back to the shock without major energy loss (at least in a 10^4 K gas). The resulting suprathermal ions typically have velocities of order 10 times the downstream thermal proton velocity and, in a 10^4 K gas without ongoing photoionization, have a charge of $Q^* \leq +3$. In a 10^6 K gas, the mean charge can be higher (i.e. $\sim +9$ for Fe) and energy losses for the sputtered ions may be significant.

It is instructive to examine where the factor of 10^{-4} comes from; two of the four decades come from the low sputtering yield per collision, one from the fact that the acceleration time scale is typically a decade longer than the time-scale for advection out of the upstream region, and one from the fact that the number density of the accelerated grains per logarithmic interval decreases as v, while $v_{\rm G,max}$ is about a decade above v_0. We note in passing that this relatively low probability

also means that the process of grain acceleration does not significantly change discussions of grain destruction and processing by shock waves, at least in the upstream region.

In view of the rather crude nature of this estimate it is remarkable that the answer appears close to what is required by the GCR composition observations. As is well known, if one simply assumes that the accelerated protons have a p^{-2} power-law spectrum from a few times thermal energy to an upper cut-off at around 10^{14} eV, the condition that the total energy flux in accelerated protons out of the shock cannot exceed the mechanical power in, implies that only about 1 in 10^4 of the incident thermal protons can become part of the cosmic ray proton power law. The coincidence of this figure with the estimate for the ion sputtering probability suggests that the resultant accelerated cosmic ray composition will be fairly close to the average chemical composition of the interstellar medium. But, since the sputtered ions are injected at a velocity about a decade higher than the protons, the refractory elements should show an enhancement which is also of order 10 (see Fig. 3.4 in Jones and Ellison 1991).

2.5. Detailed Assumptions of Monte Carlo Shock Model

In the Monte Carlo technique used here, we model a plane, parallel, steady-state shock, i.e., the angle between the upstream magnetic field and the shock normal, $\Theta_{\rm Bn}$, is assumed to be zero everywhere and the shock is taken to be an infinite plane. We mimic the curvature of a real SNR shock by placing a free escape boundary (FEB) at some distance, $d_{\rm FEB}$, upstream from the shock. Shocked particles reaching the FEB are lost from the system, thus truncating the acceleration process. We note that in the calculation of Berezhko, Elshin, and Ksenofontov (1996), the size of the SNR shock, rather than its age, also limits the acceleration process. In a steady state, with a diffusion coefficient which increases with energy, a FEB boundary is required to obtain self-consistent solutions in all but extremely low Mach number shocks (Eichler 1984; Ellison and Eichler 1984). It has been shown in Kang and Jones (1995) (see also Knerr, Jokipii, and Ellison 1996) that a FEB works in a similar fashion in time-dependent, plane shocks. Our steady-state assumption precludes a description of the overall dynamics of the SNR explosion; instead, we use standard Sedov estimates for SNR shock radii, speeds, and ages where these are required.

The Monte Carlo model makes the same assumption for the scattering mean free path as made to obtain equation (13), i.e.,

$$\lambda = \eta r_{\rm g} \ , \tag{38}$$

where η is a constant independent of particle species, energy, or position. The diffusion coefficient is then $\lambda v/3$, where v is the particle speed in the local plasma frame. Henceforth, all lengths will be measured in units of $\lambda_0 = \eta r_{\rm g1}$, where $r_{\rm g1} = m_{\rm p} V_{\rm sk}/(eB_1)$ is the gyroradius of a far upstream proton with a speed equal to the shock speed. We further assume that all particles scatter elastically and isotropically in the local plasma frame. By assuming that the scattering is elastic against a massive background, we model a situation where particles scatter against waves

which are frozen-in the plasma. This assumption ignores the possible transfer of energy between the particles and the background wave field, and will be most accurate for high Mach number shocks. Obviously, the assumption that equation (38) holds over many orders of magnitude from thermal energies to 10^{14-15} eV is a gross simplification of the complex plasma physics which controls particle diffusion in the self-generated magnetic turbulence near shocks. However, $r_{\rm g}$ is the fundamental length scale for scattering, and equation (38) does model strongly energy dependent diffusion. In addition, equation (38) has been shown to (a) be consistent with spacecraft observations of protons and heavy elements accelerated at the quasi-parallel Earth bow shock (Ellison, Möbius, and Paschmann 1990), (b) allow models of Ulysses spacecraft data of protons and He^{+2} accelerated at interplanetary traveling shocks (Baring et al. 1995), (c) be of a similar form to that determined directly from self-consistent plasma simulations (Giacalone et al. 1992,1993), and (d) match plasma simulation results for injection and acceleration when used in the Monte Carlo simulation we employ here (Ellison et al. 1993). It must be cautioned, however, that all of the above comparisons were performed in energy ranges far smaller than those modeled here; nevertheless we feel this expression for the diffusion contains the essential physics of the processes involved and allows reasonably self-consistent models, which can be meaningfully compared to observations.

We further assume the SNR shocks in question are capable of accelerating *protons* to energies on the order of $E_{\rm p,max} \sim 10^{14-15}$ eV. This limit is imposed by the observed constancy of the energetic proton spectral shape up to those energies (Shibata 1995); cutoffs above this energy can be interpreted in terms of either the finite size of the shock acceleration region (e.g. Berezhko, Elshin, and Ksenofontov 1996), or the finite age of the remnant (e.g. Prishchep and Ptuskin, 1981; Lagage & Cesarsky 1983), depending on the parameters. For our models here, we assume a finite shock size limits proton acceleration. If the waves responsible for scattering high energy particles are self-generated, the upstream diffusion length of the highest energy particles currently in the system will define the turbulent foreshock region. Energetic particles backstreaming to the limits of the foreshock region will leave the system truncating the acceleration. Since we assume that the magnetic turbulence responsible for isotropizing protons of a given gyroradius will act similarly on other species (including grains!) of the same gyroradius, the acceleration of all other species will cease when their diffusion lengths in the upstream medium, $L_{{\rm D},\alpha} = \kappa_\alpha / V_{\rm sk}$, equals that of the highest energy protons. Since $\kappa_\alpha = \lambda_\alpha v_\alpha / 3$ and $\lambda_\alpha = \eta r_{{\rm g},\alpha}$, the shocks will be able to accelerate an ion of species α up to an energy such that

$$v_\alpha p_\alpha = E_{\rm p,max} Q_\alpha \ , \tag{39}$$

or

$$\left(\frac{E}{A}\right)_{\alpha,\rm max} = \zeta \left(\frac{Q}{A}\right)_\alpha E_{\rm p,max} \ , \tag{40}$$

where $(E/A)_{\alpha,\rm max}$ is the approximate maximum kinetic energy per nucleon a species α will obtain in a shock large enough to accelerate protons to $E_{\rm p,max}$. Here $\zeta = 1$ for highly relativistic maximal energies (α = true ion, $(Q/A)_\alpha > 10^{-2}$) and $\zeta = 1/2$ for non-relativistic ones (α = grain, $(Q/A)_{\rm G} \sim 10^{-8}$). For $E_{\rm p,max} \geq 10^{14}$ eV, we get for grains $(E/A)_{\rm G,max} \geq 500$ keV, due to the finite size of the

SNR. As seen above, the energies actually reached by grains are limited to only $(E/A)_G \lesssim 100$ keV by collisional friction (§ 2.3).

In terms of the actual SNR environment, the maximum energy depends on three parameters, $d_{\rm FEB}$ which is some measure of the shock radius, η, and the magnitude of the upstream magnetic field, B_1. As long as we confine ourselves to parallel shocks, these three parameters can be combined into one. We take $d_{\rm FEB}$ to be some fraction f of the shock radius $R_{\rm sk}$, and set this distance equal to the upstream diffusion length, i.e., $fR_{\rm sk} = \kappa_1/V_{\rm sk}$. For highly relativistic particles, this gives:

$$\frac{\eta r_{\rm g} c}{3V_{\rm sk}} = fR_{\rm sk} \ , \tag{41}$$

and since

$$r_{\rm g} = \frac{A}{Q}\frac{(E/A)}{eB_1 c} \ , \qquad \text{(SI units)} \tag{42}$$

we obtain for the maximum kinetic energy per nucleon,

$$\left(\frac{E}{A}\right)_{\rm max} = \frac{Q}{A}\left(\frac{fB_1}{\eta}\right)3eR_{\rm sk}V_{\rm sk} \ . \tag{43}$$

Replacing $R_{\rm sk}$ and $V_{\rm sk}$ with their Sedov values at $t_{\rm SNR}$ we have

$$\left(\frac{E}{A}\right)_{\rm max} \simeq 3\times 10^{14}\left(\frac{Q}{A}\right)\left(\frac{fB_1}{\eta\ 3\mu{\rm G}}\right)\left(\frac{n_{\rm H}}{1\,{\rm cm}^{-3}}\right)^{-1}\left(\frac{E_{\rm SN}}{10^{51}{\rm erg}}\right)^{2/5}\left(\frac{t_{\rm SNR}}{10^3{\rm yr}}\right)^{-1/5}\ {\rm eV} \ , \tag{44}$$

or, in terms of $V_{\rm sk}$,

$$\left(\frac{E}{A}\right)_{\rm max} \simeq 2\times 10^{14}\left(\frac{Q}{A}\right)\left(\frac{fB_1}{\eta\ 3\mu{\rm G}}\right)\left(\frac{n_{\rm H}}{1\,{\rm cm}^{-3}}\right)^{-1/3}\left(\frac{E_{\rm SN}}{10^{51}{\rm erg}}\right)^{1/3}\left(\frac{V_{\rm sk}}{10^3\,\frac{\rm km}{\rm s}}\right)^{1/3}\ {\rm eV} \ . \tag{45}$$

Values of $(E/A)_{\rm max} \sim 10^{14}(Q/A)$ eV can be obtained for $f \sim 0.3$, $\eta \sim 1$ (i.e. the Bohm limit), and $B_1 \sim 3\times 10^{-6}$ G over a fairly wide range of $t_{\rm SNR}$. In the examples presented here, we arbitrary set the parameter fB_1/η so that a maximum proton energy of $\sim 10^{14}$ eV is obtained in all cases.

Unfortunately, the situation is more complicated than this since if cosmic rays carry enough energy to influence the shock structure, the shock radius and speed will, in fact, depend on the maximum energy cosmic rays obtain. However, these effects are small and will not influence the general characteristics of the solutions we obtain. In oblique shocks, there will be a far more complicated relation between η, B_1, and the shock obliquity, $\Theta_{\rm Bn}$ (e.g. Ellison, Baring, and Jones 1995). Obliquity effects may be extremely important for modeling the radio emission from young SNRs, which is observed to vary considerably around the rim of shell-like remnants (e.g., Fulbright and Reynolds 1990), and may influence cosmic ray composition if highly oblique shocks give a different ratio of heavy elements to protons than do parallel ones. However, while we have produced results for nonlinear oblique shocks at nonrelativistic energies (Ellison, Baring, and Jones 1995), we are not yet able to model nonlinear oblique shocks to the energies required here and leave this to future work.

3. NUMERICAL RESULTS

We first produce nonlinear solutions for the shock structure including the acceleration of protons and He^{+2} to energies $\sim 10^{14}$ eV. Both species are included self-consistently and contribute to the smoothing of the shock. Helium is injected far upstream from the shock at 'cosmic' abundance, i.e., $n_{He}/n_H = 0.1$. Once the shock structure has been determined, we accelerate other gases and grains as test particles in the smooth shock, including the slowing and sputtering of these grains from direct collisions with the ambient gas [i.e. equation (22)]. Once the grains have been accelerated, we determine the rate at which sputtered ions are injected into the shock and reaccelerated (as test particles) as described above and discussed in detail below.

3.1. Non-Linear Shock Models

We have tested several SNR models, including one with a high shock speed, $V_{sk} = 10^4$ km s^{-1}, typical of a young SNR at the end of the free expansion (or ballistic) stage (e.g., Drury, Aharonian, and Völk 1994) (model I), one with an intermediate speed (i.e., $V_{sk} = 2000$ km s^{-1}, model II), and one with a slow speed typical of older, slower remnants in the Sedov phase ($V_{sk} = 400$ km s^{-1}, model III). These three models, where the parameter $fB_1/(\eta\ 3\mu G)$ has been set equal to 0.2 (0.34) [0.6] for model I (II) [III] to allow acceleration of protons to $\sim 10^{14}$ eV, span a wide parameter range and show the essential effects for most supernova explosions in the ISM. In addition, we illustrate the effects a low Mach number has on the acceleration efficiency with Model IV, where $V_{sk} = 150$ km s^{-1}. In order to save computation time and improve statistics, we have used a low cutoff energy ($E_{max} \sim 10^7$ keV/nuc) and this example is not intended to be a realistic model of SNR acceleration. Model IV has $M_1 = 6.4$ and $r = 6.6$, where M_1 is the far upstream sonic Mach number.

Our solutions are obtained by iteration and the technique is described in detail in Ellison, Jones, and Reynolds (1990). In Figure 2 we show the gas flow speed in the shock frame, versus distance from the shock (i.e., the shock structure or profile, $U_x(x)$), determined by our Monte Carlo technique for models I, II, and III. Notice that the distance is plotted with a logarithmic scale for $x < -10\lambda_0$ and a linear scale for $x > -10\lambda_0$. The shock is smoothed on the diffusion length scale $\sim \kappa/V_{sk}$ of the highest energy particles in the system. Despite this extreme smoothing, a distinct subshock persists with an abrupt transition to the downstream state occurring in about one thermal ion gyroradius. While the three cases shown differ in details, they are qualitatively the same and result in similar particle spectra as discussed below.

In analyzing Figure 2, it is essential to realize that the distance unit λ_0 is proportional to V_{sk}. Since approximately the same maximum energy is obtained in each case, the precursor length in real units scales essentially as $1/V_{sk}$.

Another important point to notice in comparing the nonlinear solutions to the test particle

one (shown as a dotted line in Figure 2), is that the overall compression ratio is well above four in the nonlinear cases. As has been described before (e.g., Ellison and Eichler 1984; Jones and Ellison 1991), in steady-state shocks the overall shock compression will depend on the fraction of pressure contributed by relativistic particles and on the amount of energy flux lost at the FEB. The solutions depend on the compression ratio in a strongly nonlinear fashion and our method determines the overall compression as well as the shape of the flow profile self-consistently. The fraction of pressure that ends up in relativistic particles depends on the shock speed as well as the Mach number and this contributes to the fact that Models I and II have approximately the same compression ratios even though they differ in Mach number. A large compression ratio will result in flatter spectra and more efficient acceleration.

In Figure 3 we show differential flux spectra for models I, II, and III. The spectra are calculated in the shock frame, at a position downstream from the shock, and measured in energy per nucleon. The light solid lines are the proton spectra and the light dashed lines are the He^{+2} spectra. The proton spectra are normalized to one thermal proton injected far upstream per cm^2 per sec and thermal helium is injected far upstream with $n_{He}/n_H = 0.1$. We will discuss the grain spectra (heavy solid and dotted lines) below.

The result of shock smoothing is seen in the H^+ and He^{+2} spectra; below $\sim Am_pc^2$ ($\sim 10^6$ keV/A) the spectra curve slightly upward as the particles get more energetic. This comes about because as the particles increase in energy, they develop a longer diffusion length and 'feel' a stronger compression ratio. Around $\sim Am_pc^2$, kinematic effects cause a steepening as the particles become relativistic, but above $\sim Am_pc^2$, the upward curvature begins again. Since the highest energy particles diffuse across the full density jump, r, just below the turnover caused by the FEB the spectra develop slopes not too different from that expected from test-particle Fermi acceleration, i.e., $dJ/dE \propto E^{-\sigma}$, where $\sigma = (r+2)/(r-1)$ for relativistic energies.

3.2. Acceleration of Interstellar Gases

The fact that our calculation conserves mass, momentum, and energy fluxes, and calculates the entire distribution function, allows a direct measure of the absolute shock acceleration efficiency. Once we assume that all ion species obey equation (38), the smooth shock produces different injection and acceleration efficiencies which are increasing function of A/Q. Unfortunately, the charge state of a given sample of interstellar gas is not well known since we don't know the gas temperature, and it may be influenced by photoionization by the SN explosion UV flash, by X-rays from the hot, shocked downstream gas, or by nearby stars. In addition, the charge state of ions can change due to charge stripping during acceleration.

However, the acceleration process at low energies is rapid enough that charge stripping can be ignored in the energy range where a substantial fraction of the A/Q enhancement occurs (at least up to ~ 100 MeV/nucleon if singly charged anomalous cosmic rays are produced in a similar

fashion at the solar wind termination shock, e.g., Cummings and Stone 1996).

Therefore, if all elements start with similar charge states, the abundance of heavy ions relative to protons will be an increasing function of mass. Because of this, we believe the increase of abundance with mass seen for gas-phase elements in cosmic rays (Figure 1) is a fairly clear signature of particle acceleration in smooth shocks (e.g., Eichler 1979; Ellison 1981).

To obtain specific estimates of the abundance enhancements, we have calculated the spectra for a number of gases, all injected with the same number density far upstream from the shock and all (except H^{+1}) with a charge of +2, which remains unchanged during acceleration. A charge state of +2 might occur in the cool ISM ($\sim 10^4$ K) subjected to UV or X-ray photoionization. Figure 4 shows these spectra for Models II (top panel), III (middle panel), and IV (bottom panel) and the vertical dotted lines show where abundance ratios relative to hydrogen are calculated. The abundance ratios vary considerably between the three shock models. The high Mach number shock gives large ratios and all elements are accelerated more efficiently than protons. In the lower Mach number shocks, however, helium can actually be underabundant relative to hydrogen, simultaneously with the heavier elements being enhanced. This comes about because both the pre-shock temperature and the particle A/Q influence the injection efficiency. In high Mach number shocks, the upstream thermal speed is a small fraction of the shock speed for all ion species so the velocity increment gained in the first shock crossing is approximately equal to $U_1 - U_2$ for all species. Therefore, the efficiency is nearly monotonic in A/Q. In low Mach number shocks, however, the thermal speed becomes comparable to the shock speed and differences in the pre-shock temperature become more important. Since we inject all species at the same temperature, heavy ions have a smaller pre-shock speed than protons, both A/Q and the thermal speed are important and influence the acceleration in opposite ways, and the efficiency need not be a monotonic function of A/Q. We repeat that, for computational reason, Model IV has a lower maximum energy cutoff than the other models and is not intended to represent a realistic SNR model. We include it to emphasize the effect Mach number has on enhancement and to illustrate that the H/He ratio can be greater than one over the entire energy range (bottom panel, Figure 4). While the qualitative nature of the abundance ratios shown by Model IV are largely independent of the maximum energy, the enhancements of heavy elements are exaggerated somewhat by the low cutoff energy which produces a larger compression ratio than would be the case if a higher cutoff was used (see Ellison & Reynolds 1991 for details).

While the ratios are energy dependent and the relative abundances of the heavy ions continues to increase relative to hydrogen beyond 1 GeV/A (for Models II and III), in reality, charge stripping during the longer acceleration times at higher energies will progressively reduce the A/Q values at higher energies. We expect this effect to become dominant around 100-1000 MeV/A, and assume that the high energy enhancements are roughly those calculated for constant $Q = +2$ at these energies (vertical dotted lines in the top two panels of Figure 4). Clearly, the rules we have just stated for determining the abundance ratios, constant $Q = +2$, ratios calculated at 100-1000 MeV/A, ignoring enhancements that occur at higher energies, are somewhat arbitrary and other assumptions could be made; however, none would qualitatively change the results.

The abundance ratios determined from Figure 4 are compared to the gas-phase element cosmic ray observations in Figure 5. The dotted lines are from Model II ($V_{\rm sk} = 2000$ km s^{-1}) and the dot-dashed lines are from Model III ($V_{\rm sk} = 400$ km s^{-1}); in each case, the upper line is calculated at 1 GeV/A, the lower line is calculated at 100 MeV/A, and the value for hydrogen is set to one. The two averages from the dotted and dot-dashed lines are shown in Figure 1 with a slight renormalization. Despite the uncertainties involved for the charge state and other approximations, it's clear that the shock model does an excellent job of reproducing the abundances of gas-phase elements in cosmic rays. The general increase with mass is reproduced as is the magnitude of the abundance enhancement relative to hydrogen (we note that a similar relationship was obtained by Ellison 1981). Even the fact that the observed H/He ratio is actually more in cosmic rays than in the Sun (see Paper I) can be naturally accounted for if the shocks producing the bulk of the cosmic rays are of sufficiently low Mach numbers, as shown by Model IV in Figure 4.

We also note that exceptions to the general increase of abundance with mass may occur, as with carbon, oxygen, and ^{22}Ne, if an additional source of material (i.e., Wolf-Rayet stars; see paper I) is present. In such a case, the abundance will lie *above* our predictions. Our estimate for the non-Wolf-Rayet abundance of cosmic ray carbon is indicated in Figure 1.

3.3. Grain Sputtering and Abundances of Refractory Cosmic Rays

Having determined abundances for cosmic ray gas-phase elements, we now determine the abundance of cosmic ray refractory elements from ions sputtered off grains. Clearly this is a very complicated problem since grains come in many sizes, with varied compositions, and largely unknown structures. Our aim here is to obtain quantitative results by making simple, straightforward assumptions and approximations for grain and shock properties. This will show the plausibility that refractory element cosmic rays originate in grains and we leave to later work more complex models.

In our model, the same shock which accelerates interstellar gases will simultaneously accelerate dust grains. In Figure 3, the heavy solid lines are test-particle 'grain' spectra for grains with our standard parameters, i.e., $a = 10^{-7}$ m, $\phi = 10$ V, and $\mu = 56$ (yielding $A/Q \simeq 8 \times 10^7$). The grains have been accelerated in the smooth shocks shown in Figure 2. They have undergone losses from collisions with the gas and the high energy turnover reflects the situation where the loss time approximately equals the acceleration time. This should be compared to equation (26). Note that we take $B_1 = 3 \times 10^{-6}$ G and $n_{\rm H} = 1$ cm^{-3} here and in all of the examples below. The test-particle grains were injected with $n_{\rm G} = n_{\rm H}$ and must be scaled by the actual ambient thermal grain density to obtain the absolute normalization (i.e., $n_{\rm G}/n_{\rm H} \sim 3 \times 10^{-14}$).

The enhancement effect for large A/Q particles is clearly seen in the grain spectra. While the grains were injected with the same number density as protons, they obtained a much flatter spectrum at low energies resulting in a substantial enhancement before their spectra cut off. As they accelerate, the grains sputter and ions sputtered off in the upstream region will be further

accelerated upon convecting into the shock. We model this by including in the Monte Carlo simulation a direct determination of $I(v)$ during grain acceleration and then perform a separate run using $I(v)$ as the injection rate of grain products. In reality, this reacceleration would occur simultaneously with the grain and gas acceleration.

Since the Monte Carlo code follows individual particles, we know the time spent in the upstream region, the position of the particle, its speed, and the background density at that position. We find $I(v)dv$ by multiplying the sputtering rate, $0.01 n_{\rm H}(x) a^2 v_{\rm G}$, by the time and summing the number of sputtered atoms produced in each velocity bin. We neglect all ions sputtered downstream from the shock since a sputtered ion has an A/Q ratio many orders of magnitude smaller than its parent grain, which means it is many more mean free paths downstream from the shock than the parent grain. We sum over the entire upstream region assuming, as before, that all upstream sputtered ions are injected into the shock without losses. In this way we obtain $I(v)$, the number of injected ions per unit area per unit time with speeds between v and $v + dv$.

When $I(v)$ is injected and accelerated, we obtain the results shown with heavy dotted lines in Figure 3. Here we have assumed that the sputtered ions have $A = 56$ and $Q = 2$, but show below the effect of varying this charge. Again, the sputtered ion spectra must be scaled down by the actual ambient grain density since we have injected the grains with $n_{\rm G} = n_{\rm H}$. The most striking feature in Figure 3 is that the sputtered product flux lies many orders of magnitude above the grain flux. This comes about mainly because each grain contains $\sim 10^9$ iron atoms, so that even a small fraction ($\sim 10^{-3}$) of sputtered ions will make up a large flux of accelerated ions. An additional increase comes in because the sputtered products with $A/Q = 56/2$ are accelerated more efficiently than the protons or alphas. Charge stripping during acceleration will lower this enhancement somewhat.

The injection rates, $I(v)$, for the three examples of Figure 3, still normalized to $n_{\rm G} = n_{\rm H}$, are shown in Figure 6. As described in Section 2.4.1, $I(v)$ peaks strongly just below the grain cutoff energy and we use this fact to approximate the injection of grain erosion products as a δ-function at the weighted mean energy of $I(v)$. The actual sputtered ion injection energies per nucleon, $E_{\rm inj}/A$ and rates, $f_{\rm inj}$, used in Figure 3 are labeled in Figure 6.

The acceleration of grains and sputtered products is an extremely complicated process with a number of factors influencing the final cosmic ray abundance. These factors include: the size, charge, and mean molecular weight of the grain, the background gas density, the collision and sputtering rate, any losses sputtered ions experience before being further accelerated, and the charge state of the sputtered ion including charge stripping before and during acceleration. In addition, shock properties, such as the Mach number, shock age, geometry, ambient magnetic field strength, and maximum proton energy obtained, will modify the resultant cosmic ray abundance. Since many of these factors are poorly known, it is impossible to precisely predict the refractory cosmic ray abundance. However, we can investigate some of these factors to see how robust the process is.

In Figure 7 we show results for grains of various sizes. We have used Models I ($V_{\rm sk} = 10^4$ km s^{-1}) and III ($V_{\rm sk} = 400$ km s^{-1}) and the lower eight panels show the low energy portion of the proton spectra (light lines) with 'grain' spectra (heavy lines) of sizes, $0.001 < a < 1\mu$m, all injected with the same far upstream number density as protons and all including losses by collisions with the background gas. We have kept all other parameters constant and equal to those of Figure 3, i.e., $\mu = 56$, $\phi = 10$ V, $B_1 = 3 \times 10^{-6}$ G, and $n_{\rm H} = 1$ cm^{-3}. Several important effects are illustrated by these plots. The top two panels, labeled $A/Q = 2$, show a comparison between protons and helium (we repeat that in these plots all species are injected with the same far upstream number density) and there is barely any enhancement effect for helium over protons. However, as a and A/Q increase, the slope of the distribution flattens and the enhancement becomes quite large. For each horizontal pair of panels, the A/Q values shown are obtained from equation (8) using the grain size labeled in each panel. It is also clear from this figure that as A/Q is increased, the enhancement reaches a maximum (at any given energy per nucleon) and then falls off for larger A/Q. At some point (e.g., $a \sim 1\mu$m for Model I and $a > 1\mu$m for III), the grain size becomes large enough that the grains essentially only cross the shock once before being lost downstream. For some grain sizes, the enhancement over protons is more than a factor of 100 at a few MeV/A and this will translate into the efficient production and acceleration of sputtered ions. The important point is that significant enhancement of grains occurs for sizes spanning at least three orders of magnitude in radius (i.e., more than six orders of A/Q) for very different shock speeds ranging from $V_{\rm sk} = 400$ to 10^4 km s^{-1} indicating that the effect is quite robust. It is clear, however, that very small or very large grains will not be enhanced by this process. The results for Model II lie between those shown.

Another aspect of the grain acceleration evident in Figure 7 is that as A/Q is increased, the downstream quasi-thermal peak shifts to higher energy per nucleon (the quasi-thermal peak is made up of ions or grains that have crossed the shock only once). This effect also comes about because of the smooth shock. If the shock were discontinuous, all spectra would show the thermal peak at approximately the same energy per nucleon, the only difference coming from differences in upstream thermal speeds which will be quite small for high Mach numbers. However, in the smooth shock, larger A/Q particles get a larger velocity kick on their first crossing of the shock. For $V_{\rm sk} = 10^4$ km s^{-1} (Model I), the velocity kick received for $A/Q \sim 10^8$ grains is approximately five times that for $A/Q = 1$.

We now make specific assumptions for the shock and grain properties in order to obtain a direct estimate of the cosmic ray abundance of iron. Our predictions, of course, will depend on the particular assumptions we make. We assume that *all* iron which ends up as cosmic rays originates in grains. Using our 400 km s^{-1} shock Model III, we inject and accelerate grains with $a = 0.1\mu$m, $\phi = 10$ V, $\mu = 56$, assuming $B_1 = 3 \times 10^{-6}$ G, and $n_{\rm H} = 1$ cm^{-3}. We next assume that all sputtered iron ions are swept back into the shock without significant energy losses. Furthermore, we assume that in the 100–1000 years or so they spend convecting back to the shock [i.e., equation (29)], they become fully stripped as seems likely. The Fe^{+26} ions are then re-accelerated in the same shock which accelerated the grains.

Our results are shown in Figure 8 and compared to the proton spectrum (light and heavy solid lines). The accelerated grains are shown with a dashed line, and sputtered Fe ions are shown with dotted lines. The test-particle grains are injected far upstream with solar (i.e., "cosmic") abundance, that is, the total number of Fe *atoms* in the grains is $\sim 3.1 \times 10^{-5}$ times the number of H atoms. This means that the ratio of far upstream number densities is $n_{\rm G,Fe}/n_{\rm H} \sim 3 \times 10^{-14}$ since, for $a = 0.1\mu$m, there are $\sim 10^9$ Fe atoms per grain. In order to indicate the difference the sputtered ion charge state makes, we show Fe spectra for Fe^{+2} (i.e., without stripping), as well as Fe^{+26}. In the actual case, there will be a mixture of charge states since sputtered ions formed close to the shock will be convected back before much charge stripping can occur. These ions will be accelerated more efficiently than the Fe^{+26} ions, but fully stripped ions obtain a higher maximum energy per nucleon in the finite size shock. On the other hand, sputtered ions will experience some ionization energy losses before encountering the shock which will cause them to be accelerated less efficiently. In want of a more complete model, we compare the Fe^{+26} spectrum with no upstream losses to the observations in Figure 9 below.

In any event, it is clear from this figure that a large enhancement of iron over protons occurs. Between $\sim$ 10 and 100 GeV/A, the sputtered Fe^{+2} ions stand about a factor of 10^3 above their solar abundance relative to hydrogen and the Fe^{+26} stands about a factor of 20 above (compare the light solid proton line, which has been divided by the cosmic abundance of Fe, to the heavy dotted lines). In the next section we compare these predictions, both normalization and spectral shape, to observed cosmic ray spectra.

3.4. Spectral Comparisons

In Figure 9 we compare our proton, helium, and Fe^{+26} spectra to cosmic ray observations. The data in Figure 9 is adapted from the compilation of cosmic ray observations presented by Shibata (1995). Both data and model spectra have been multiplied by $(E/A)^{2.5}$ to flatten the steep spectra.

In addition, since we compare with observed spectra, we must correct our calculated source spectra for rigidity dependent escape from the galaxy and reduction due to nuclear destruction. Evidence, including the comparison of secondary to primary element spectra, indicate that cosmic rays escape from the galaxy at a rate proportional to some power of the rigidity, i.e. $R^{-\delta}$ at relativistic energies (e.g., Protheroe, Ormes, & Comstock 1981; Engelmann et al. 1990; Shibata 1995). While the actual escape may be more complicated than this and the exponent may vary somewhat with different galactic propagation models and/or energy, this form is sufficient for our purposes considering other uncertainties in our model. With this assumption, the ratio of the observed flux to the source flux for a species α is

$$\frac{\Phi_{\alpha,\rm obs}}{\Phi_{\alpha,\rm s}} \propto R^{-\delta} \ . \tag{46}$$

If we consider only relativistic particles and compare fluxes of species α to protons we have,

$$\left(\frac{\Phi_{\alpha,\rm obs}}{\Phi_{\alpha,\rm s}}\right)\Big/\left(\frac{\Phi_{\rm p,obs}}{\Phi_{\rm p,s}}\right) = \left(\frac{\Phi_{\alpha,\rm obs}}{\Phi_{\rm p,obs}}\right)\Big/\left(\frac{\Phi_{\alpha,\rm s}}{\Phi_{\rm p,s}}\right) = \left(\frac{R_\alpha}{R_{\rm p}}\right)^{-\delta} = \left(\frac{A_\alpha}{Q_\alpha}\right)^{-\delta} \quad \text{at equal } \frac{E}{A}\ , \tag{47}$$

and

$$= (Q_\alpha)^{\delta} \quad \text{at equal } E \text{ per nucleus}\ . \tag{48}$$

Thus, at fully relativistic energies, identical source spectra in energy per nucleon will show He^{+2} lower by a factor $2^{-\delta}$ after energy dependent escape from the galaxy. If additionally, protons are 10 times more numerous in the source gas than helium nuclei, the observed helium flux will be $2^{-\delta}/10$ as intense as the proton flux assuming both are accelerated with the same efficiency.

We have corrected the helium and iron fluxes for nuclear destruction using for the surviving fraction, $1/[1+(\lambda_e/\lambda_d)]$, where λ_e is the rigidity dependent escape length and the nuclear destruction length, λ_d, is 2.7 g cm^{-2} for iron and ~ 35 g cm^{-2} for elemental helium.

For the comparison in Figure 9, we have used Model III ($V_{\rm sk} = 400$ km s^{-1}) and our results for protons are shown as a solid line and those for He^{+2} with a dashed line. The model source spectra have been multiplied by $R^{-0.65}$ and helium has been corrected for nuclear destruction, although this is a small effect for helium. The rigidity dependence we have chosen, $\delta = 0.65$, is close to the best value, $\delta = 0.6$, adopted by Engelmann et al. (1990) and Shibata (1995). If reacceleration during propagation is important, δ could go down to 0.3 (e.g., Berezinskii et al. 1990).

Several features are evident in Figure 9. First of all, solar modulation is not included in our model and its effect shows in the data which fall off somewhat below the kinematic turnover near 1 GeV/nucleon. Second, our model matches the gross features of the spectra extremely well above the energy where modulation is important and below where our model spectra fall off from the effects of our adopted finite size SNR shock. We must caution that the fit to the slope depends strongly on the value for δ we choose and should not be over interpreted. Cosmic rays undoubtedly come from a number of supernovae of varying sizes, Mach numbers, etc., and a model such as ours of a single shock is not intended to model the observations in complete detail. Our Models I and II, with larger compression ratios, produce even flatter spectra than Model III and either would not fit the spectral observations or would fit only with a larger value of δ. In addition, they would predict H/He ratios that are too low. Having said this, we wish to emphasize while we have adjusted the overall normalization of the *proton* spectrum to match the observations, there is *no adjustment of the relative normalization* between protons and helium. Our 400 km s^{-1} shock model, using the cosmic abundance of helium, reproduces the observed relative fluxes fairly accurately. The fact that our model yields a H/He ratio somewhat lower than observed, may imply that lower speed shocks are important (see Figures 4 and 5). Lastly, the proton and helium spectra from the nonlinear model show a slight upward curvature indicative of nonlinear shock acceleration.

The heavy dotted line in Figure 9 shows the Fe^{+26} curve from Figure 8 multiplied by $(E/A)^{2.5} \times R^{-0.65}$ and corrected for nuclear destruction. Once these corrections are made, the normalization

relative to protons is exactly that shown in Figure 8, i.e., the iron is injected out of a medium with solar abundance $n_{\rm Fe} = 3.1 \times 10^{-5} n_{\rm H}$ and the model sets the abundance relative to hydrogen. Clearly, the excellent match to the observed normalization is somewhat fortuitous considering the many uncertainties in the model. However, we have chosen parameters we feel to be realistic and demonstrated that the grain model is quite robust; we do not expect that this result will fundamentally change as refinements are made. The light dotted line shows the Fe^{+26} spectrum without the nuclear destruction correction which tends to remove the otherwise distinctive curvature expected from nonlinear shock acceleration. Without this correction, the non-power law nature of the spectrum is more pronounced and, in fact, we predict that this curvature is real and sufficiently accurate cosmic ray observations may reveal it.

Our prediction for the source cosmic ray iron abundance is included in Figure 1. To give some indication of the errors intrinsic to our calculation, we show two horizontal lines on the right side of the plot. The lower line is the ratio, Fe^{+26}/H^{+}, taken at 100 GeV/A in Figure 8, and the upper line is taken at 10 GeV/A. The match is excellent. The same enhancements should apply roughly for the other refractory elements in Figure 1 since, in the crucial early acceleration phase, they are all accelerated, not as individual ions, but as constituents of the same grains.

The obvious failure of our model to produce spectra above $\sim 10^6$ GeV is one that all models using single, isolated SNRs have. While parameters can be chosen to extend the maximum energy up above 10^{16} eV, it has been known since Lagage and Cesarsky (1983) that *standard* parameters for shock acceleration and SNRs yield a maximum energy below the observed knee in the cosmic ray spectrum and far below the highest energy cosmic rays. More elaborate models involving explosions into the pre-supernova stellar wind may be able to account for cosmic rays up to and beyond the knee (see Völk and Biermann 1988; Biermann 1993).

4. SUMMARY AND DISCUSSION

4.1. GCR Source Composition; Volatility Versus FIP

We have presented a one-site, one-step model of galactic cosmic ray (GCR) origin and acceleration that produces cosmic ray source spectra with slopes and relative abundances which match observations. In this scenario, GCRs come from interstellar or circumstellar gas and dust grains accelerated simultaneously by SNR shocks. Our model combines an acceleration of the gas-phase, volatile elements with an A/Q dependent enhancement, and a preferential acceleration of the grains, and hence of the sputtered, refractory elements initially locked in them.

In addition to accounting for the general excess of the standard low first ionization potential (FIP) refractory elements, this scenario can account naturally for a number of the long-standing puzzles in the GCR source composition (see Paper I): (i) The low H, He, and N abundances, relative to heavier elements (A/Q effect); (ii) The currently assessed low Na/Mg, Ge/Fe, Pb/Pt, and the

high P/S ratios (grain acceleration effect); (iii) The weak mass-dependence of the refractory element enhancements, as opposed to the strong mass-dependence of the enhancements for the volatiles (since the refractory elements are first accelerated, not as individual ions, but as constituents of grains); (iv) The apparent general overabundance of ultra-heavy elements beyond $Z \sim 60$ or even ~ 40, if it is confirmed (A/Q effect); and (v) The presence of ^{22}Ne, C, and O enhancements in GCRs, which comes naturally from the contribution of the most massive SNae, which accelerate their own ^{22}Ne–^{12}C–^{16}O enriched pre-SN Wolf-Rayet wind material.

Our predictions are summarized in Figure 1. The dotted, dot-dashed, and solid curves show our predictions for highly volatile cosmic ray abundances as a function of mass (in a specific ionization model) for shock velocities of 2000, 400, and 150 km s^{-1}, respectively. The somewhat high H/He ratio observed suggests a significant contribution of lower Mach number shocks. The horizontal solid lines give our estimates for refractory element (i.e. iron) GCRS abundance, which is more or less independent of mass. We interpret the elements with intermediate volatility as coming from a mixture of gas and dust in the ISM.

Specifically, we predict that: (i) All gas-phase elements accelerated out of ISM or circumstellar matter with normal composition will have abundances which lie in the range given by the dotted and dot-dashed lines shown in Figure 1. Based on the observed ^{22}Ne excess, we expect an additional source of carbon and oxygen from the acceleration of ^{12}C–^{16}O–enriched Wolf-Rayet wind material affected by He-burning nucleosynthesis, causing these elements to lie *above* the line by the amount contributed by this additional source. Our estimate for the non-Wolf-Rayet carbon contribution is labeled in Figure 1; it could represent an overestimate if a significant fraction of carbon is not in the gas phase (as we assumed), but locked in grains in the C–rich Wolf-Rayet wind material (C/O > 1), and hence preferentially accelerated. (ii) Refractory elements such as iron, magnesium, silicon, etc., which are essentially locked in dust grains in the ISM, will be accelerated preferentially relative to the gas-phase elements, and will have GCRS abundances determined by grain properties and gas-grain interactions, such as mean grain size, sputtering rates, etc. However, we have shown that the preferential acceleration of heavy grains is not strongly dependent on these properties. So, all refractories should end up with abundances independent of condensation temperature and mass, and not too far from our prediction for iron. (iii) No significant amount of SN ejecta material is being accelerated, in view of the minor role played by the short-lived reverse shock, and of the low probability that fast blobs of ejecta material overtake the forward shock. (iv) Cosmic ray spectra (at energies above those where solar modulation is important) will not be strict power laws, but will show a concave upward curvature distinctive of nonlinear shock acceleration. (v) The shock acceleration of interstellar grains will produce grain speeds relative to the background plasma considerably greater ($\beta_G \sim 0.01$) than is generally assumed. While only a small fraction of the total number of grains will obtain these maximum speeds, the bulk of the grains will be shock heated to ∼keV/A energies (see Figure 3). This may result in important modifications to the X-ray modeling of the shock wave environment, and may explain recent observations of a broad ^{26}Al γ-ray line. The width of the 1.809-MeV γ-ray emission line seen by GRIS (Naya et al. 1996),

implies that ^{26}Al decay occurs at speeds > 450 km s^{-1}, or at energies per nucleon of ~ 1 keV/A. If the ^{26}Al is locked in grains with large rigidities, shocks with speeds somewhere between our Models II and III (see Figure 3), will produce grain distributions consistent with these results.

For many years, the GCR source composition has been interpreted in terms of a FIP fractionation, similar to that extensively observed in the solar environment, but usually without considering the possibility of an A/Q dependence of the acceleration efficiency (Meyer 1985; see, however, Silberberg and Tsao 1990). One may wonder whether a FIP fractionation, combined with an A/Q dependent bias reflecting acceleration conditions, could account for the composition data as convincingly as our volatility model. This hypothesis would equally well explain the strong mass dependence of the high-FIP (volatile) element enhancements, but we do not see how it could simultaneously account for the lack of a comparable, strong mass-dependence of the low-FIP (refractory) element enhancements. Indeed, in any FIP scenario the particles have to be accelerated out of an already FIP-biased gas, resulting from a prior ion-neutral fractionation; in this gas, all elements, whatever their FIP, have to be at least singly ionized to get accelerated, so that low- and high-FIP elements no longer behave differently (cf., e.g., solar energetic particles accelerated out of FIP-biased 10^6 K coronal gas; e.g. Meyer 1985, 1993). The combined FIP and A/Q hypothesis cannot account for the low Na/Mg, Ge/Fe, Pb/Pt, and high P/S ratios since two elements of comparable FIP and mass are being compared in each of these ratios. Furthermore, FIP scenarios require a two-stage acceleration mechanism, in two different sites (acceleration to MeV energies in later-type star environments; combined with acceleration to GeV and TeV energies by SN shock waves), and the Wolf-Rayet star source for the ^{22}Ne-C-O excess has to be treated as a totally separate component (Meyer 1985). So, in our current view, the great similarity[3] between the GCR source composition (volatility-biased, due to preferential acceleration of grain material), and the solar coronal, solar wind, and solar energetic particle composition (FIP-biased, due to an ion-neutral fractionation in the $\sim 10^4$ K solar chromosphere) is purely coincidental!

4.2. Other Non-Linear Shock Acceleration Models

While we believe ours is the first attempt to give a detailed description of grain and gas acceleration in nonlinear shocks, a great deal of work on nonlinear acceleration of protons (and some including other atomic species) has been done (for reviews, see Blandford and Eichler 1987; Berezhko and Krymsky 1988; Jones and Ellison 1991). The work that is closest to ours has been presented in a series of papers by Berezhko and co-workers (Berezhko, Yelshin, and Ksenofontov 1994; Berezhko, Ksenofontov, and Yelshin 1995; Berezhko, Elshin, and Ksenofontov 1996), but see Kang, Jones, & Ryu (1992), and Kang & Jones (1995, 1996) for similar nonlinear shock work. Berezhko et al. couple the diffusive transport equation describing the cosmic ray distribution

[3]The similarity is actually not complete since Na and P seem to be less abundant in the GCRs than in solar energetic particles (Garrard & Stone 1993; Reames 1995; paper I).

function to the background fluid described by gas dynamic equations with the cosmic ray pressure added in. This is much the same as done in Drury, Aharonian, and Völk (1993) and a number of previous investigations (see above reviews). However, unlike most previous analytic studies, Berezhko et al. have been able to develop techniques which allow them to use a strongly energy dependent diffusion coefficient. As done here, they assume that the scattering mean free path is proportional to the gyroradius, but set $\kappa = r_g c/3$ for simplicity, neglecting the change in particle speed at nonrelativistic energies. They determine the fraction of the total ejecta energy going into cosmic rays as a function of time, and calculate the overall spectrum of cosmic rays during the evolution of the remnant, including adiabatic losses as the high density region near the shock expands to the ISM value. The result is a spectrum which is quite similar to a power law in momentum over the entire range from thermal to $\sim 10^{15}$ eV, and with about 20% of the ejecta energy going into cosmic rays.

One major difference between their work and ours is that they have a time-dependent model and are, therefore, able to follow the evolution of the shock and the SNR dynamics, whereas we are restricted to a steady-state, and do not calculate the overall remnant dynamics. However, they conclude that geometric factors, i.e., particle escape from the finite sized shock, limit the maximum energy obtained in the shock. This fact makes our steady-state model more applicable than would be the case if remnant age limited acceleration.

Another important difference between our model and those based on the diffusion equation is that the diffusion approximation (i.e., the requirement that particle speeds be large compared to flow speeds) limits the ability to treat particle injection. For example, Berezhko et al. must assume that some small fraction, ϵ, of the incoming gas is transferred to cosmic rays, and the overall efficiency with which cosmic rays are produced, $E_{\rm cr}/E_{\rm SN}$, depends critically on ϵ. In Berezhko, Ksenofontov, and Yelshin (1995), $E_{\rm cr}/E_{\rm SN}$ is shown to vary from about 0.2 for $\epsilon \simeq 10^{-4}$ to about 0.8 for $\epsilon \simeq 10^{-3}$ for a shock with an initial Mach number of about 30.

In contrast, our Monte Carlo description is not restricted to superthermal particles, and once we assume that all particles obey equation (38), injection is treated self-consistently. There may be questions concerning the appropriateness of equation (38), but once such a scattering description has been chosen, both the injection rate and the injection momentum are fully determined by the solution, for all species, without any additional parameters such as ϵ. In contrast, Berezhko, Elshin, and Ksenofontov (1996) must make two additional assumptions to treat species other than protons. The first is that all species obtain the same thermal velocity distribution *behind* the shock, and the second is an ad hoc enhancement factor, $e(A/Q) = R^\beta$, added to the injection rate, where β is a free parameter chosen to match cosmic ray abundance observations.

4.3. Future Work

The current study provides a framework that seems qualitatively capable of accounting for all the features of the observed composition within a single acceleration context. Much work is required to substantiate it, and to ensure that it can apply in the real supernova (SN) shock wave environment. In particular, a number of points will have to be investigated for the various stellar masses contributing SNae, according to their weight in the initial mass function and to their efficiency in accelerating particles. These include: (i) The nature of the external material accelerated by the shock. This is presumably local ISM for the lower mass SNae, and pre-SN stellar wind for the more massive ones (including the Wolf-Rayet stars responsible for the ^{22}Ne-C-O enhancements); (ii) The ionization states present in this external material. It could be 10^6 K material, in which refractory grain cores would not have been evaporated; it cannot be collisionally ionized 10^4 K material, in which Ne and He would be mainly neutral, but it could be 10^4 K photoionized material, e.g., by the UV burst associated with the SN explosion, or by an X-ray precursor associated with the shock wave. The more precise relationship between A/Q and A for the volatile elements should be, as much as possible, investigated in the various hypothesis; (iii) The origin of the grains, which could be those formed recently in the pre-SN stellar wind for the massive SNae, or old ISM grains for the lower mass ones. The grain composition may be different for grains newly formed in stellar winds, in which T_c could be the essential parameter, and for old ISM grains, where slow chemical reprocessing should be important as well (e.g., Jones et al. 1994; Draine 1995); in the old ISM, phosphorus, in particular, seems less locked in grains than expected based on its rather high T_c, which is not consistent with its presumably high GCRS abundance; this might represent a hint that circumstellar dust is important in the GCR sources (e.g., Savage and Sembach 1996; Paper I); (iv) The expected excesses of ^{22}Ne, C, and O associated with the contribution of the most massive, WC and WO Wolf-Rayet star SNae should be more precisely evaluated, as well as the, certainly much smaller, excess of nitrogen associated with WN Wolf-Rayet stars; note that the carbon excess (Figure 1) might be due, in addition to Wolf-Rayet star nucleosynthesis, to a significant fraction of carbon being condensed into solid form in C-rich Wolf-Rayet atmospheres (C/O $>$ 1), where *not all* C is prevented from condensing by CO formation (e.g. van der Hucht and Williams 1995). For more details, see Paper I; (v) The determination of the relative contribution of SNRs with various shock strengths in order to simultaneously account for both the systematic increase of the enhancement with mass among the volatile elements and the somewhat high H/He ratio.

5. CONCLUSIONS

A re-analysis of the observed galactic cosmic ray chemical composition (especially Na, P, Ge, and Pb; Paper I) strongly suggests that cosmic ray source material consists mainly of two components both originating in the interstellar medium (and/or circumstellar material): volatile elements from the gas-phase, and refractory elements from dust grains. Relative to solar abundances, the

abundances of the volatile elements are found to be a strongly increasing function of mass with the sole exception of hydrogen. In contrast, the abundances of the refractory elements, known to be locked in grains in the ISM, are systematically higher, but with little or no mass dependence, allowing a clear separation of these components in the data. The elements which are likely to be *partly* locked in grains in the ISM show up midway between these two groups. This evidence points to separate injection and/or acceleration processes depending on whether an element is mainly in the gas-phase or in dust in the ISM.

We have shown here that standard nonlinear shock acceleration theory can account for these composition features. We assume that supernova remnant blast waves moving through the undisturbed ISM or circumstellar matter pick up and accelerate gas ions and dust grains simultaneously. The gaseous ions are accelerated directly to cosmic ray energies in the smoothed shock, which produces an enhancement of high mass/charge (i.e. A/Q) elements. Since heavier elements always tend to have higher A/Q ratios, the mass dependence seen in the volatile cosmic ray abundances is a clear signature of acceleration by smoothed shocks. This accounts, in particular, for the low cosmic ray hydrogen and helium abundances relative to heavier volatile elements; the somewhat high cosmic ray H/He ratio suggests a significant contribution of low Mach number shocks in the acceleration process, consistent with the estimated source spectral shapes. If we assume that the weakly charged, massive grains act in the ambient magnetic fields exactly as protons of the same rigidity, these grains will be very efficiently accelerated by the same shocks, although up to far lower energy per nucleon ($\sim$ 100 keV/nucleon) than the gas ions, due to friction and to the limited age and size of the SNR. By including a simple model of the sputtering of these grains upstream from the shock, and the acceleration of the sputtered ions to GeV and TeV cosmic ray energies, we are able to calculate the relative abundances of refractory elements to volatile ones. In view of the crucial role of the injection stage in shaping the composition, this injection of refractory elements as constituents of entire grains results in a lack of a significant mass dependence of the refractory element abundances, as observed.

So, the elements originating in gas and dust are both accelerated by the same shocks, but have different abundances in cosmic rays because they have different injection routes; gas-phase elements are directly picked out of the thermal plasma and accelerated, while grain material is first accelerated as entire grains, the grains are then subjected to sputtering, and finally the sputtered ions are further accelerated, in the same shock, to cosmic ray energies. The relative abundances of refractory to gas-phase elements is determined by grain physics such as the sputtering rate, average grain size, etc., and is found to be consistent with observations.

It is important to note that, if our model is correct, the long standing belief that cosmic rays accelerated to GeV and TeV energies by SNR shock waves were first injected to MeV energies with appropriate coronal gas composition by later-type stars, is rejected. This belief was based almost solely on the fact that solar energetic particle and galactic cosmic ray abundances show a similar correlation with first ionization potential (FIP). This similarity is now assumed to be coincidental, stemming from the fact that there is a strong correlation for most elements between volatility and

FIP. We also note that our one-step, one-site model is much simpler than any scenario based on stellar injection processes, which involve two acceleration stages in two unrelated sites. Our process also accounts naturally for the relative deficiency of the two most abundant species, hydrogen and helium, and can account, without recourse to a different type of source, for the ^{22}Ne–C–O excess observed in galactic cosmic rays; this excess comes from the most massive star SN shocks, which are bound to accelerate their own ^{22}Ne–^{12}C–^{16}O–enriched pre-SN Wolf-Rayet star wind material.

The model we have presented is far from complete. We have used a plane, steady-state model to mimic a curved, evolving supernova remnant. Further, grain properties are sufficiently unknown that fairly large uncertainties exist for typical grain sizes and sputtering rates, and we have made no attempt to model SNRs developing in interstellar or circumstellar media with different parameters. We also must assume that grains interact with the background magnetic field nearly elastically, as is believed to be the case for gas ions. All of these and other uncertainties need to be investigated. However, we believe the striking ordering of the cosmic ray composition data in terms of refractory and volatile elements (Figure 1) is a compelling reason to require that interstellar grains be accelerated by shock waves.

It is also clear that we fail to explain cosmic rays with energies above the knee at $\sim 10^{15}$ eV, and that our spectra are somewhat flatter than required by some propagation models. These problems, however, are common to any model based on an isolated supernova exploding in the ISM (e.g., Berezhko, Elshin, and Ksenofontov 1996), and have nothing to do with the acceleration of grains.

D. Ellison and L. Drury wish to acknowledge the hospitality of the Service d'Astrophysique, Centre d'Etudes de Saclay where much of this work was carried out. L. Drury's visit was supported by the Commission of the European Communities under contract ERBCHRXCT940604, and D. Ellison was supported, in part, by the NASA Space Physics Theory Program, the Service d'Astrophysique, the Observatoire de Paris-Meudon, and CNET/CETP (Issy-les-Moulineaux). The authors also thank T. Shibata for kindly furnishing recent cosmic ray data, and K. Borkowski, T. Gaisser, S. Reynolds, and D. Reames for helpful discussions.

REFERENCES

Axford, W.I. 1981, in Proc. 17th ICRC(Paris), 12, 155

Axford, W.I., Leer, E., & Skadron, G. 1977, in Proc. 15th ICRC(Plovdiv), 11, 132

Baring, M.G., Ogilvie, K.W., Ellison, D.C., & Forsyth, R. 1995, Adv. Space Res., 15, 385

Baring, M.G., Ogilvie, K.W., Ellison, D.C., & Forsyth, R. 1997, Ap. J., in press

Bell, A.R. 1978, M.N.R.A.S., 182, 147

Berezhko, E.G., Elshin, V.K., & Ksenofontov, L.T. 1996, JETP , 82, 1

Berezhko, E.G., & Krymsky, G.F. 1988, Usp. Fiz. Nauk. 154, 49 (English translation, Sov. Phys. Usp. 31, 27)

Berezhko, E.G., Ksenofontov, L.T., & Yelshin, V.K. 1995, Nucl. Phys. B (Proc. Suppl., 39A, 171

Berezhko, E.G., Yelshin, V.K., & Ksenofontov, L.T. 1994, Astroparticle Phys., 2, 215

Berezinskii, V.S., Bulanov, S.V., Dogiel, V.A., Ginzburg, V.S., & Ptuskin, V.S. 1990, Astrophysics of Cosmic Rays, North-Holland, Amsterdam

Bibring, J.P., & Cesarsky, C.J. 1981, in Proc. 17th ICRC(Paris), 2, 289

Biermann, P.L. 1993, A.A., 271, 649

Blandford, R.D., & Eichler, D. 1987, Phys. Repts., 154, 1

Blandford, R.D., & Ostriker, J.P. 1978, Ap.J.(Letts), 221, L29

Bode, M.F. 1988, in Dust in the Universe, M.E. Bailey & D.A. Williams eds., (Cambridge University Press), p. 73

Cardelli, J.A. 1994, Science, 265, 209

Cesarsky, C.J., & Bibring, J.P. 1980, in IAU Symp. No. 94, G. Setti, G. Spada, & A.W. Wolfendale eds., (Kluwer), p. 361

Cesarsky, C.J., Rothenflug, R., & Cassé, M. 1981, in Proc. 17th ICRC(Paris), 2, 269

Cummings, A.C., & Stone, E.C. 1996, Space Sci. Rev., 78, 117

Draine, B.T. 1995, Astr. Sp. Sci., 233, 111

Draine, B.T., & Salpeter, E.E. 1979, Ap.J., 231, 77

Drury, L. O'C. 1983, Rep. Prog. Phys., 46, 973

Drury, L.O'C., Aharonian, F.A., & Völk, H.J. 1994, A.A., 287, 959

Drury, L. O'C. & Keane, A. J. 1995, Nucl. Phys. B 39A 165

Dwek, E. 1987, Ap.J., 322, 812

Dwek, E., Moseley, S.H., Glaccum, W., Graham, J.R., Loewenstein, R.F., Silverberg, R.F., & Smith, R.K. 1992, Ap.J.(Letts), 389, L21

Eichler, D. 1979, Ap.J., 232, 106

Eichler, D. 1984, Ap.J., 277, 429

Ellison, D.C. 1981, Ph.D. Thesis, The Catholic University of America

Ellison, D.C. 1993, in Proc. 23rd ICRC(Calgary), 2, 219

Ellison, D.C., Baring, M.G., & Jones, F.C. 1995, Ap.J., 453, 873

Ellison, D.C., & Eichler, D. 1984, Ap.J., 286, 691

Ellison, D.C., Giacalone, J., Burgess, D., & Schwartz, S.J. 1993, J.G.R., 98, 21,085

Ellison, D.C., Jones, F.C., & Eichler, D. 1981, J. Geophys., 50, 110

Ellison, D.C., Jones, F.C., & Eichler, D. 1983, in Proc. 18th ICRC(Bangalore), 2, 271

Ellison, D.C., Jones, F.C., & Reynolds, S.P. 1990, Ap.J., 360, 702

Ellison, D.C., Möbius, E., & Paschmann, G. 1990, Ap.J., 352, 376

Ellison, D.C., & Reynolds, S.P. 1991, Ap.J., 382, 242

Engelmann, J.J., Ferrando, P., Soutoul, A., Goret, P., Juliusson, E., Koch-Miramond, L., Lund, N., Masse, P., Peters, B., Petrou, N., & Rasmussen, I.L. 1990, A.A., 233, 96

Epstein, R.I. 1980, M.N.R.A.S., 193, 723

Fulbright, M.S., & Reynolds, S.P. 1990, Ap.J., 357, 591

Garrard, T.L., & Stone, E.C. 1993, in Proc. 23rd ICRC(Calgary), 3, 384

Gehrz, R.D. 1991, in Interstellar Dust, IAU Symp. No. 135, L.J. Allamandola & A.G.G.M. Tielens eds., (Kluwer, Dordrecht), p. 445

Giacalone, J., Burgess, D., Schwartz, S.J., & Ellison, D.C. 1992, G.R.L., 19, 433

Giacalone, J., Burgess, D., Schwartz, S.J., & Ellison, D.C. 1993, Ap.J., 402, 550

Jackson, J.D. 1962, Classical Electrodynamics, John Wiley & Sons, New York

Jones, F.C., & Ellison, D.C. 1991, Space Sci. Rev., 58, 259-346

Jones, A.P., Tielens, A.G.G., Hollenbach, D.J., & McKee, C.F. 1994, Ap.J., 433, 797

Jun, B.-I., & Norman, M.L. 1996, Ap.J., 472, 245

Kang, H., & Jones, T.W. 1995, Ap.J., 447, 944

Kang, H., & Jones, T.W. 1996, Ap. J., in press

Kang, H., Jones, T.W., & Ryu, D. 1992, Ap.J., 385, 193

Knerr, J., Jokipii, R.J., & Ellison, D.C. 1996, Ap.J., 458, 641

Koyama, K., Petre, R., Gotthelf, E.V., Matsuura, M., Ozaki, M., & Holt, S.S. 1995, Nature, 378, 255

Krymsky, G.F. 1977, Soviet Phys. Dokl., 22, 327

Lagage, P.O., & Cesarsky, C.J. 1983, A.A., 125, 249

Lang, K.R. 1980, Astrophysical Formulae, Springer-Verlag, New York, p. 302

Lucy, L.B., Danziger, I.J., Gouiffes, C., & Bouchet, P. 1989, in Supernovae, S.E. Woosley ed., (New-York: Springer), p. 82

Lucy, L.B., Danziger, I.J., Gouiffes, C., & Bouchet, P. 1991, in Structure and Dynamics of the Interstellar Medium, IAU Coll. No. 120, G. Tenorio-Tagle, M. Moles & J. Melnick eds., (New-York: Springer), p. 164

Mathis, J.S., Rumpl, W., & Nordsieck, K.H. 1977, Ap.J., 217, 425

McKee, C.F., Hollenbach, D.J., Seab, C.G., Tielens, A.G.G.M. 1987, Ap.J., 318, 674

Meyer, J.P. 1985, Ap.J.Suppl., 57, 173

Meyer, J.P. 1993, in Origin and Evolution of the Elements, Eds. N. Prantzos, E. Vangioni-Flam, & M. Cassé, Cambridge University Press, p. 26

Meyer, J.P., Drury, L. O'C., & Ellison, D.C. 1997, submitted to Ap.J. [Paper I]

Naya, J.E., Barthelmy, S.D., Bartlett, L.M., Gehrels, N., Leventhal, M., Parsons, A., Teegarden, B.J., & Tueller, J. 1996, Nature, 384, 44

Prishchep, V. L. & Ptuskin, V. S. 1981, Astron. Zh. 58, 779 (English translation Sov. Astron. 25, 446)

Protheroe, R.J., Ormes, J.F., & Comstock, G.M. 1981, Ap.J., 247, 362

Reames, D.V. 1995, Adv. Space Res., 15, (7), 41

Reynolds, S.P. 1988, in Galactic and Extragalactic Radio Astronomy, ed. G.L. Verschuur & K.I. Kellermann (Berlin: Springer), p. 439

Reynolds, S.P. 1996, Ap.J.(Letts), 459, L13

Reynolds, S.P., & Ellison, D.C. 1992, Ap.J.(Letts), 399, L75

Ryter, C., Reeves, H., Gradsztajn, E., & Audouze, J. 1970, A.A., 8, 389

Savage, B.D., & Sembach, K.R. 1996, Ann. Rev. Astr. Ap., in press

Sembach, K.R., & Savage, B.D. 1996, Ap.J., 457, 211

Silberberg, R., & Tsao, C.H. 1990, Ap.J.(Letts), 352, L49

Shibata, T. 1995, Rapporteur Talk, 24th ICRC, (Rome), in press

Shu, F.H. 1992, Gas Dynamics, Vol II, University Science Books, Mill Valley, Ca

Spitzer, L. 1962, Physics of Fully Ionized Gases, Interscience Publishers, New York

Spitzer, L. 1978, Physical Processes in the Interstellar Medium, John Wiley & Sons, New York

Swordy, S. 1993, in Proc. 23rd ICRC(Calgary), Invited, Rapporteur & Highlight Papers, p. 243

van der Hucht, K.A., & Hidayat, B. (eds.), 1991, Wolf-Rayet Stars and Interrelations with Other Massive Stars in the Galaxy, IAU Symp. No. 143 (Kluwer, Dordrecht)

van der Hucht, K.A., & Williams, P.M. (eds.), 1995, Wolf-Rayet Stars : Binaries, Colliding Winds, Evolution, IAU Symp. No. 163 (Kluwer, Dordrecht)

Völk, H.J. 1984, in High Energy Astrophysics, Proc. 19th Rencontre de Moriond, ed. Tran Than Van (Gif-sur-Yvette: Editions Frontières), p. 281

Völk, H.J., & Biermann, P.L. 1988, Ap.J.(Letts), 333, L65

Fig. 1.— Galactic cosmic ray source abundance relative to solar abundance versus atomic mass number. All values are measured relative to cosmic ray hydrogen at a given energy per nucleon. The elements are divided, on the basis of condensation temperature, into refractories, semi-volatile, volatile, and highly volatile groups. The refractories are essentially completely locked in grains in the ISM, while the highly volatile elements are gaseous. The arrows on carbon and oxygen indicate that these elements have an additional source from ^{22}Ne-C-O-enriched Wolf-Rayet wind material. Our estimate for the non-W-R contribution of carbon is labeled. Our predictions for the abundances of volatile elements from a high Mach number shock model are shown as a dotted line, and for a lower Mach number model with a dot-dashed line. The horizontal solid lines on the right side of the plot are limits on our predicted abundance of iron and other refractory elements. The label on the abscissa [$\sim (A/Q)^{\alpha}$, where α is some unspecified constant] is a reminder that, for most ionization models, A/Q is a roughly monotonically increasing function of the mass. We note that the abundances of Kr, Xe, Mo, Ba, Ce, Pt, and Pb relative to Fe may contain systematic errors which are difficult to evaluate (we indicate this with a '?' to the right of the point). For a complete discussion of the observations, see Meyer, Drury, & Ellison (1997) (Paper I).

Fig. 2.— Average bulk flow speed in the shock frame, $U_{\rm x}(x)$, versus distance (i.e., the shock structure) obtained from the Monte Carlo model. The distance scale is logarithmic for $x < -10\lambda_0$ and linear for $x > -10\lambda_0$. The vertical scale is in units of the far upstream speed, $V_{\rm sk}$, and $\lambda_0 = \eta r_{\rm g1}$, where $r_{\rm g1}$ is the gyroradius of a far upstream proton with a speed equal to the shock speed, which varies for each model. The compression ratios, r, in these nonlinear models depend on the fraction of pressure carried by relativistic particles and on the amount of energy escaping at the upstream free escape boundary (FEB) and are always greater than the standard Rankine-Hugoniot value. The dotted line shows a test-particle profile of a shock with $r = 4$. Note that even though the nonlinear shocks are smoothed on the length scales of the highest energy particles in the system, a well defined subshock remains in all cases. Our steady-state, plane-shock model is such that the profiles are constant behind the shock (i.e. $x > 0$).

Fig. 3.— Differential flux spectra in energy per nucleon obtained from shocks with $V_{\rm sk} = 10^4$ km s^{-1} (Model I), $V_{\rm sk} = 2000$ km s^{-1} (Model II), and $V_{\rm sk} = 400$ km s^{-1} (Model III). The light solid curves are the proton spectra, the light dashed curves are He^{+2} spectra, the heavy solid curves are "Fe grain" spectra, and the heavy dotted lines are Fe ions sputtered off the grains. In all models, the far upstream proton flux is normalized to one particle per cm^2 per sec, $n_{\rm He}/n_{\rm H} = 0.1$ far upstream from the shock, and the grains are test particles and are injected far upstream with the same number density as protons. At energies below the fall off produced by frictional losses, grains experience a large enhancement over protons at least in Models II and III. All spectra here and elsewhere are calculated in the shock frame at a position downstream from the shock. Note that the grain quasi-thermal peak decreases in energy per nucleon both absolutely and relative to the proton quasi-thermal peak as the shock speed decreases. This reflects the fact that in all cases the grains feel essentially the entire shock density jump and obtain an energy per nucleon of $\sim m_{\rm p} V_{\rm sk}/2$ after one shock crossing, whereas the protons obtain a quasi-thermal peak determined

by the subshock strength.

Fig. 4.— Differential flux spectra multiplied by $(E/A)^{1.5}$. All spectra are normalized to one far upstream particle injected per cm^2 per second and are obtained using smooth shock profiles. The shock structures of Models II (top panel) and III (middle panel) are shown in Figure 2. The vertical dotted lines (Models II and III) show the energy per nucleon where the abundance ratios shown in Figure 5 are calculated. For computational reasons, Model IV has a lower maximum cutoff energy than the other models. The low cutoff energy results in a high compression ratio which causes the enhancements of heavy elements to be larger than would be the case if a higher cutoff energy was used (see Ellison & Reynolds 1991 for details).

Fig. 5.— Volatile galactic cosmic ray source abundance relative to solar abundance (open circles) versus atomic mass number. As in Figure 1, the observed values are measured relative to cosmic ray hydrogen at a given energy per nucleon. Our estimate for the non-W-R contribution of carbon is labeled. The model predictions, which assume a constant charge state of +2 for the gaseous elements, are shown as dotted lines (Model II, $V_{\rm sk} = 2000$ km s^{-1}) and dot-dashed lines (Model III, $V_{\rm sk} = 400$ km s^{-1}). In each case, the upper line was calculated at 1 GeV/A, the lower line was calculated at 100 MeV/A, and the value for hydrogen was set to one. These two energies bracket the range where we believe charge stripping will produce similar A/Q's for all heavier ions which precludes further preferential acceleration. For comparison, we also show the refractory cosmic ray abundances (solid dots) to emphasize that gas-phase elements and refractories can be cleanly separated in the observations.

Fig. 6.— Injection rates for the superthermal sputtered Fe ions, $I(v)$, versus energy obtained from the grain spectra shown in Figure 3. The rates peak strongly just below the cutoff from direct losses allowing a δ-function approximation with the labeled values for the injection of the sputtered products shown in Figure 3.

Fig. 7.— Differential flux spectra in energy per nucleon. In all cases, the light line is the low energy portion of the proton spectrum shown in Fig. 3. The heavy lines show grain spectra for various grain sizes, a, for each horizontal pair of panels except for the top. The A/Q values are calculated for $\phi = 10$ V and $\mu = 56$. Model I has a shock speed, $V_{\rm sk} = 10^4$ km s^{-1}, while Model III has $V_{\rm sk} = 400$ km s^{-1}. The results for Model II are intermediate to these.

Fig. 8.— The heavy solid line shows the same proton spectrum as shown in the right-hand panel of Figure 3. The light solid line is this proton spectrum multiplied by 3.1×10^{-5}, i.e., scaled to the solar Fe/H ratio. The dashed line shows the grain spectrum normalized to the cosmic abundance of iron, i.e., the far upstream grain number density, $n_{\rm G} = 3.1 \times 10^{-5} n_{\rm H}/10^9$ cm^{-3}, where there are 10^9 iron atoms per grain. The two dotted lines show the spectra of the accelerated sputtered iron ions assuming constant charge states of +2 and +26. Note that for either charge state, the sputtered iron ends up with a flux greater than its cosmic abundance would suggest. We consider the Fe^{+26} flux the most realistic.

Fig. 9.— Cosmic ray spectra in energy per nucleon. The cosmic ray data are from the compilation of Shibata (1995) and have been multiplied by $(E/A)^{2.5}$ to produce nearly flat spectra above ~ 1 GeV/A. Note that in addition to being multiplied by $(E/A)^{2.5}$, the three source model curves (protons, solid line; He^{+2}, dashed line; Fe^{+26}, dotted lines) have been multiplied by $R^{-0.65}$ to mimic rigidity dependent escape from the galaxy and corrected for nuclear destruction during propagation. In the model, both helium and iron are injected at solar abundance, i.e., $n_{\rm He}/n_{\rm H} = 0.1$ and $n_{\rm Fe}/n_{\rm H} = 3.1 \times 10^{-5}$. The normalization of the model proton spectrum is varied to match the observations but the relative normalization of helium to hydrogen and iron to hydrogen is fixed by the model. The light dotted line shows the iron spectrum without correction for nuclear destruction. The apparent differences in spectral shape between the uncorrected iron and the other model spectra, at fully relativistic energies, are mainly the result of poor statistics.

Fig. 1

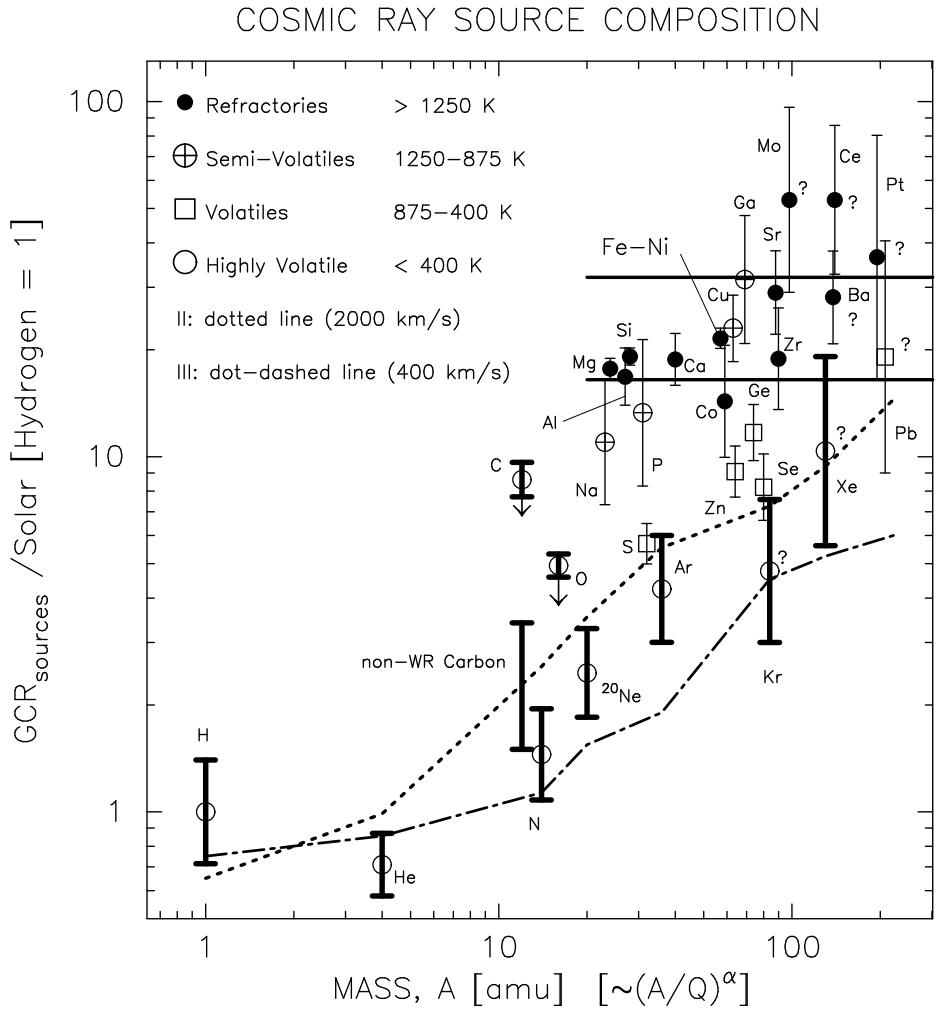

Ellison, Drury, & Meyer 1997

pt_gr_comp_mass4.com

Fig. 2

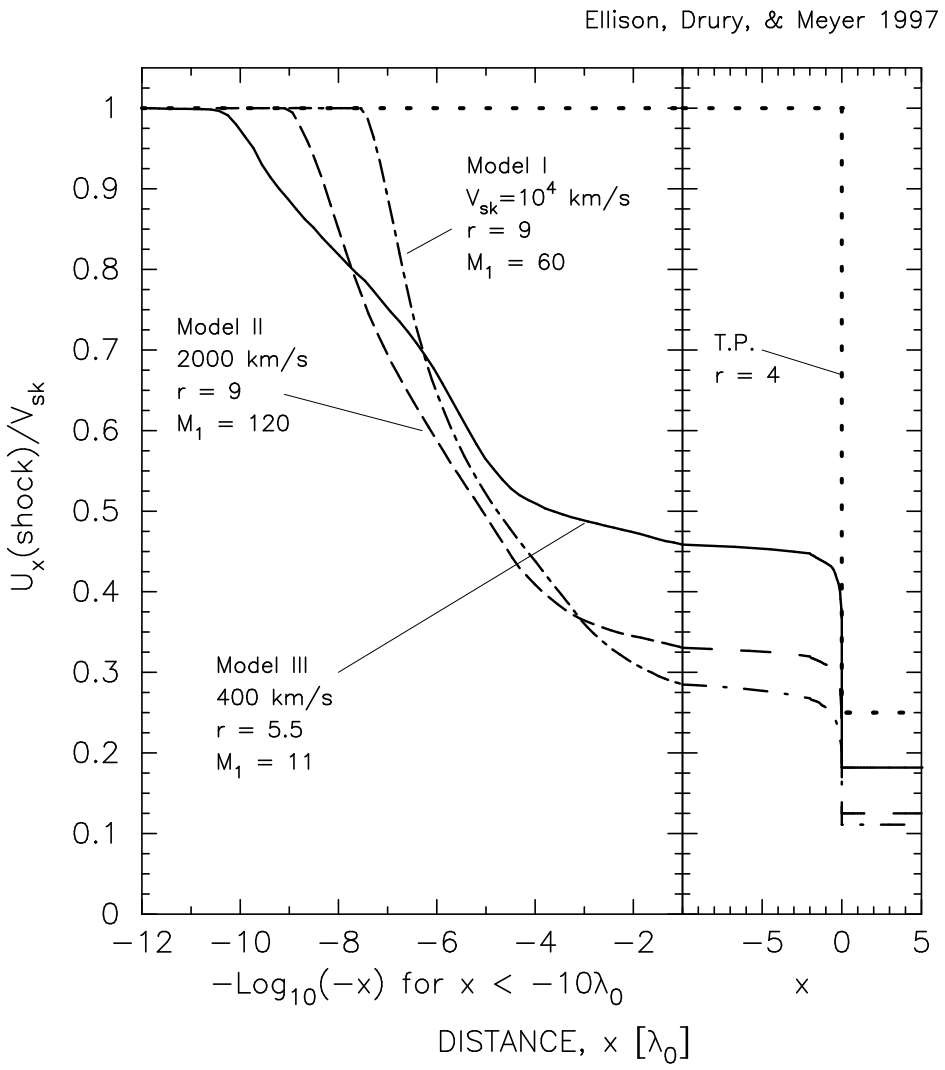
Ellison, Drury, & Meyer 1997
Model I
$V_{sk}=10^4$ km/s
r = 9
M_1 = 60
Model II
2000 km/s
r = 9
M_1 = 120
Model III
400 km/s
r = 5.5
M_1 = 11
T.P.
r = 4
U_x(shock)/V_{sk}
$-\mathrm{Log}_{10}(-x)$ for $x < -10\lambda_0$
x
DISTANCE, x [λ_0]
pt_gr_flow.com

Fig. 3

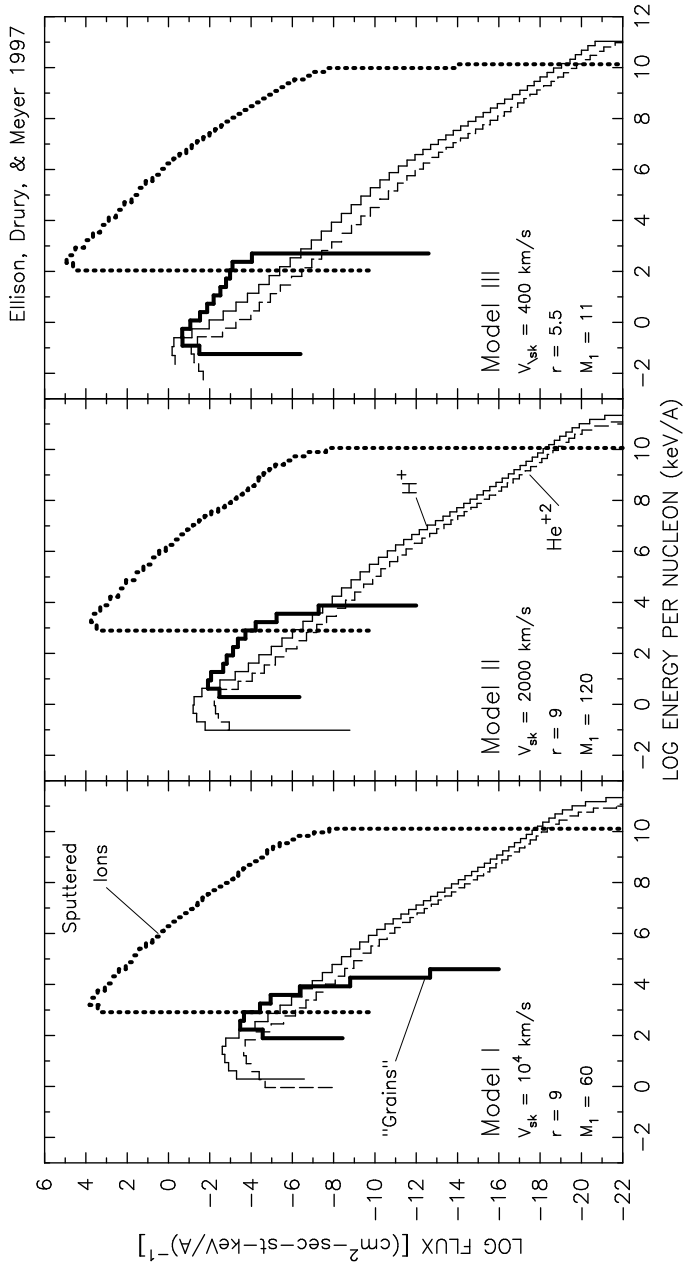

pt_gr_spec_gr.com

Fig. 4

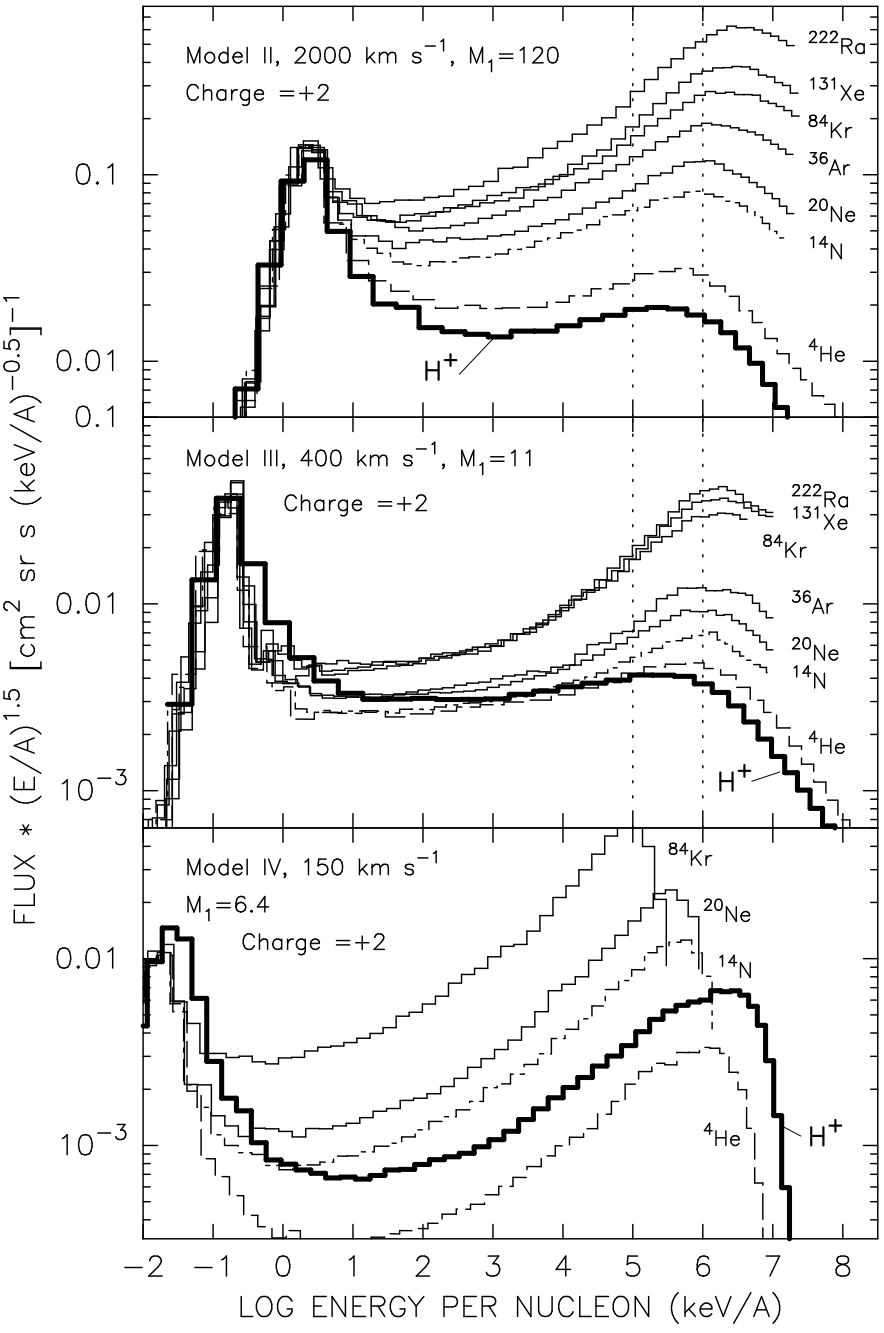

Ellison, Drury, & Meyer 1997

pt_gr_az_flat3.com

Fig. 5

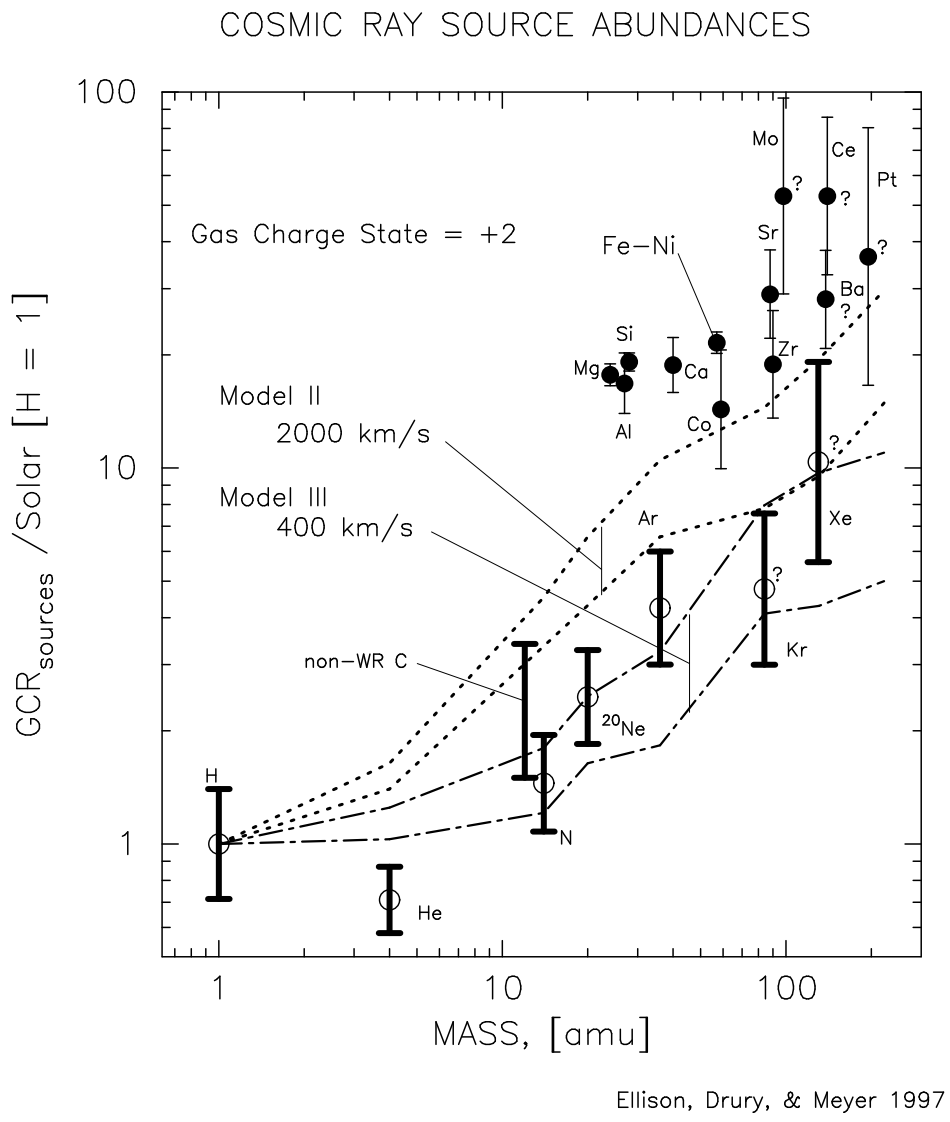

Ellison, Drury, & Meyer 1997

pt_gr_az_ratio3.com

Fig. 6

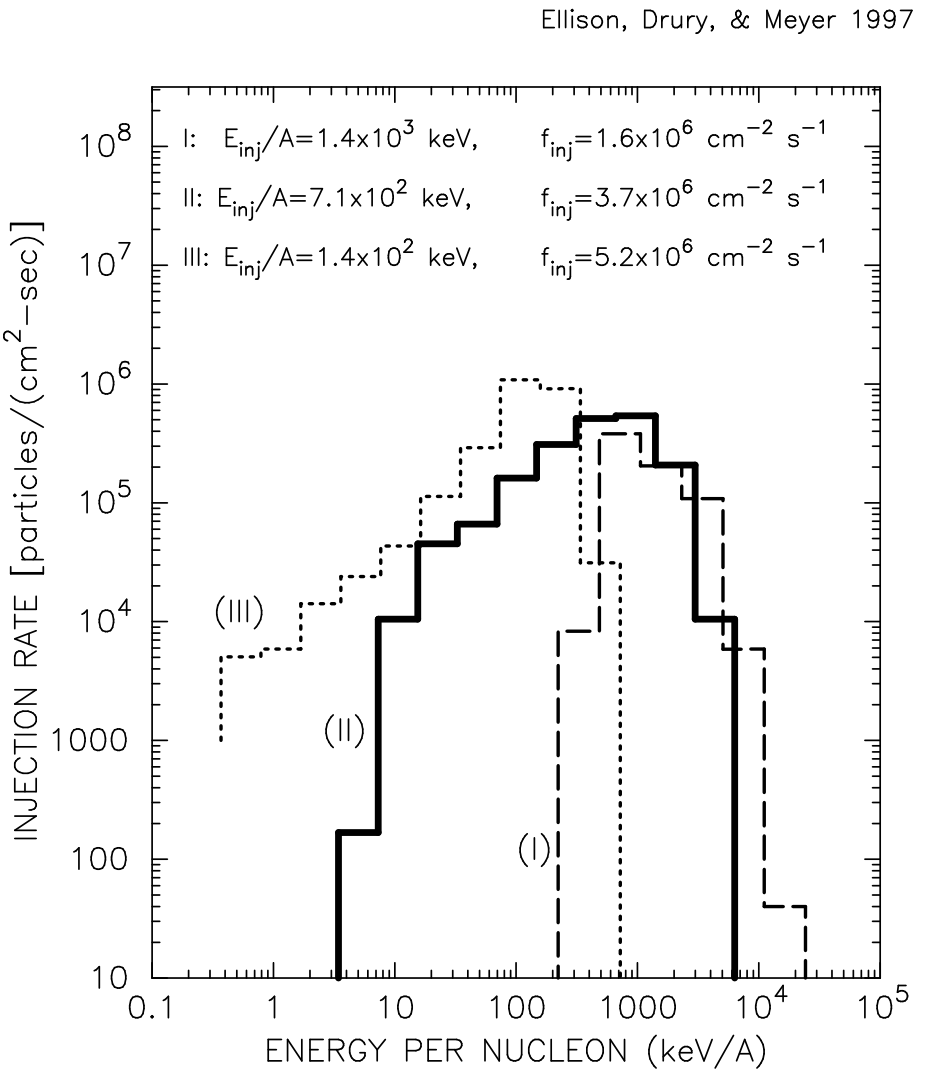
Ellison, Drury, & Meyer 1997
I: $E_{inj}/A=1.4x10^3$ keV, $f_{inj}=1.6x10^6$ cm^{-2} s^{-1}
II: $E_{inj}/A=7.1x10^2$ keV, $f_{inj}=3.7x10^6$ cm^{-2} s^{-1}
III: $E_{inj}/A=1.4x10^2$ keV, $f_{inj}=5.2x10^6$ cm^{-2} s^{-1}
(III)
(II)
(I)
INJECTION RATE [particles/(cm^2-sec)]
ENERGY PER NUCLEON (keV/A)
10
100
1000
10^4
10^5
10^6
10^7
10^8
0.1
1
10
100
1000
10^4
10^5
pt_gr_inj_rate.com

Fig. 7

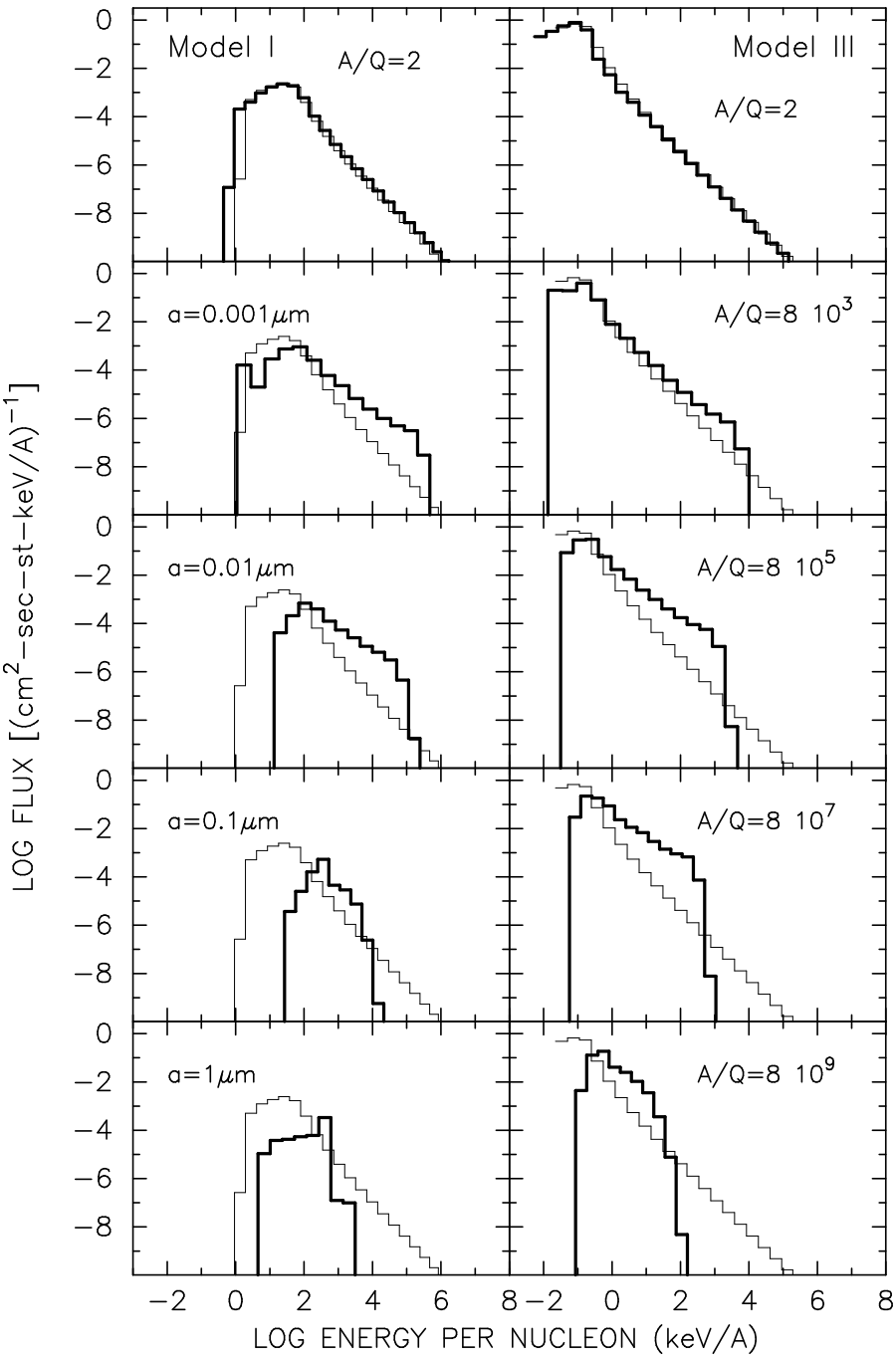

Ellison, Drury, & Meyer 1997

pt_gr_stack.com

Fig. 8

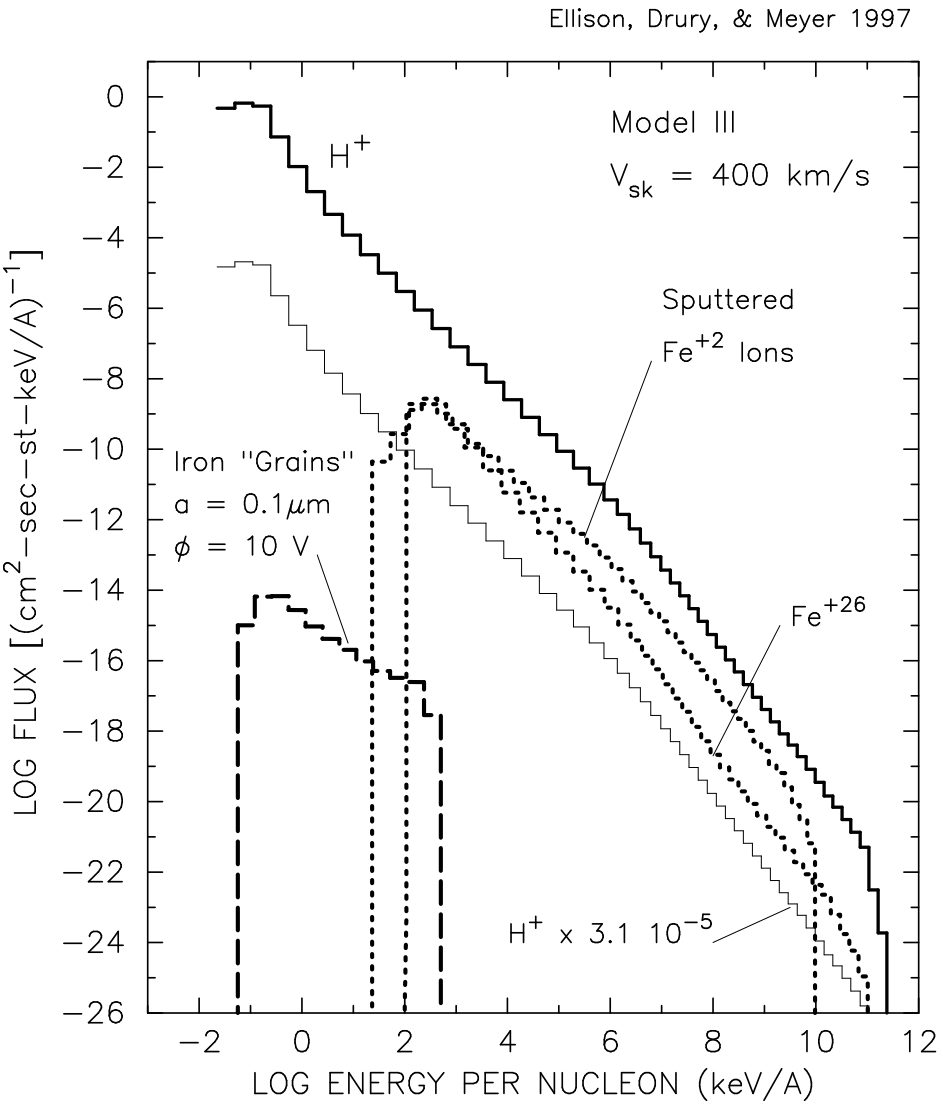

pt_gr_iron_2.com

Fig. 9

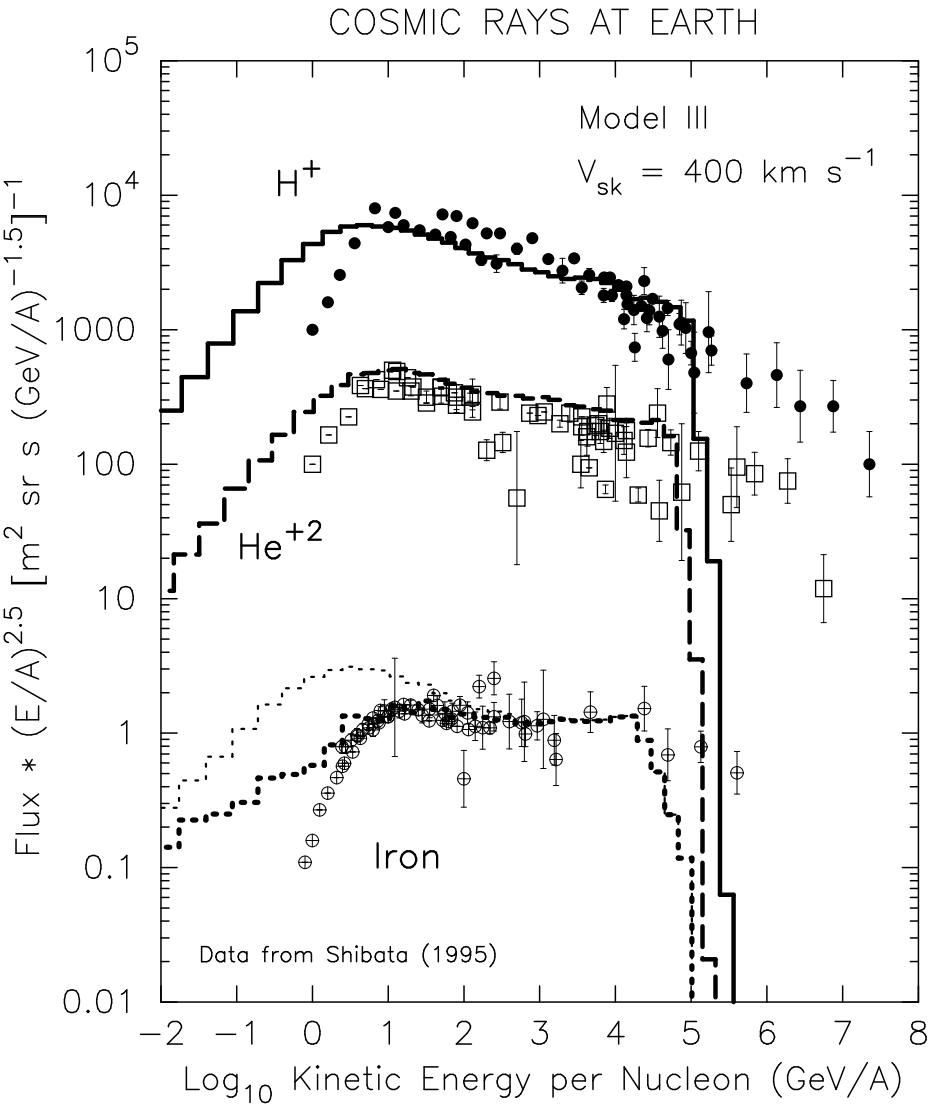

Ellison, Drury, & Meyer 1997

pt_gr_cr_EpA.com